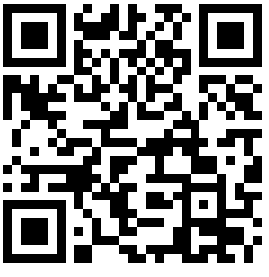

TECHNICAL REPORT S-69-3

A MODEL STUDY OF DYNAMICALLY LOADED SQUARE FOOTINGS ON DRY SAND

by

J. K. Poplin

March 1969

Sponsored by

Defense Atomic Support Agency
NWER Subtask RSS3210
and
Office, Chief of Engineers
U. S. Army
Project No. 1T022601A091-02

Conducted by

U. S. Army Engineer Waterways Experiment Station
CORPS OF ENGINEERS
Vicksburg, Mississippi

ARMY-MRC VICKSBURG, MISS.

FOREWORD

This report describes and presents the results of a model study of dynamically loaded square footings on dry sand. Basic details of test procedures and of the collection, evaluation, and interpretation of experimental data are published separately as Appendixes A through J in a supplement to this volume. Only a limited number of copies of the supplement were published; however, interested readers can borrow a copy on 30-day loan from the Research Center Library, Waterways Experiment Station.

The investigation was conducted in the Soils Division of the U. S. Army Engineer Waterways Experiment Station under the joint sponsorship of the Defense Atomic Support Agency (Nuclear Weapons Effects Research Subtask RSS3210, Response of Buried Structures to Ground Shock) and the Office, Chief of Engineers, U. S. Army (Effects of Nuclear Weapons Project No. 1-T-0-22601-A-091-02, Development of Design Criteria for Foundations of Army Protective Structure), during the period September 1964 to March 1966. The tests were conducted and the report was prepared under the direct supervision of Messrs. J. G. Jackson, Jr., and P. F. Hadala and the general direction of Messrs. W. J. Turnbull, A. A. Maxwell, and R. W. Cunny. The test program was planned and the data were analyzed by Mr. J. K. Poplin. Laboratory testing was conducted under the supervision of Mr. R. C. Sloan, assisted by Messrs. H. T. Parsons (now deceased) and R. E. Manning. SP 4 L. A. Brower, Jr. (formerly of the Waterways Experiment Station) and Mr. P. L. Marsicano conducted data-processing operations necessary for the study.

This report was prepared by Mr. Poplin. It is essentially the same, except for the placement of certain portions in the supplementary volume, as his thesis submitted to the Graduate Faculty of North Carolina State

University at Raleigh in partial fulfillment of the requirements for the degree of Doctor of Philosophy in Civil Engineering.

COL Alex G. Sutton, Jr., CE, COL John R. Oswalt, Jr., CE, and COL Levi A. Brown, CE, were Directors of the Waterways Experiment Station during the conduct of this investigation and preparation of this report. Mr. J. B. Tiffany was Technical Director.

TABLE OF CONTENTS

TABLE OF CONTENTS (Continued)

SUPPLEMENT*

LIST OF TABLES

* Published as a separate volume in a limited edition; loan copies available from Research Center Library, Waterways Experiment Station.

LIST OF FIGURES

NOTATION

Symbol	Definition	Dimensions
A	Hyperbolic constant for static reaction-displacement curve (Equation 6) (1/A is non-dimensional initial stiffness)	D
b	Width of square footing	L
B	Hyperbolic constant (Equation 6) (1/B is non-dimensional ultimate strength)	D
C_d	Depth factor coefficient (Equation 8)	D
d	Depth of burial of footing	L
g	Acceleration of gravity	LT^{-2}
G	Cone penetration resistance gradient	FL^{-3}
J	Static preload on footing prior to dynamic test	F
$k_{1,2...5}$	Constants in empirical load-time relations (Equations 11', 12', 13', 11'', 13'')	Unspecified
m	Structural mass (mass of load column)	$FL^{-1}T^2$
n	Length scale factor--ratio of length in prototype to length in model	D
p_o	Peak overpressure on prototype	FL^{-2}
P	Live load (time-dependent)	F
P_{max}	Peak dynamic load	F
q_{ud}	Ultimate bearing capacity of footing at some depth below surface (Equation 8)	FL^{-2}
q_{uo}	Ultimate bearing capacity of footing on surface (Equation 8)	FL^{-2}
R	Footing reaction, including preload (time-dependent)	F

R_{max}	Peak reaction	F
$R_{max} - J$	Peak dynamic reaction	F
R_s	Reaction to static loading	F
$R(z)$	Reaction-displacement function	F
t	Time variable (with parentheses denotes time-dependency of function)	T
$t(z_{max})$	Time of maximum footing displacement	T
T_o	Load pulse (positive phase) duration	T
T_r	Load rise time	T
u	Pore pressure	FL^{-2}
v_{avg}	Average velocity of footing	LT^{-1}
v_{max}	Maximum velocity of footing	LT^{-1}
x	Distance from center of model footing to lateral boundary of specimen	L
z	Dynamic footing displacement (time-dependent)	L
z_{max}	Maximum dynamic displacement	L
z_s	Footing displacement under static loading	L
β	Time-distortion factor due to mass distortion	D
γ	Effective unit weight of soil	FL^{-3}
γ_d	Dry unit weight of soil	FL^{-3}
ρ	Mass density of soil	$FL^{-4}T^2$
σ	Normal stress on a plane within soil	FL^{-2}
τ_f	Shear stress at failure (shear strength) on a plane within soil	FL^{-2}
ϕ	Apparent angle of internal friction	D

SUMMARY

The investigation reported herein was undertaken to develop an approach to modeling displacements of surface and shallow-buried footings on dry sand subject to high-intensity, single-pulse loads. A hypothetical shallow-buried structure with an isolated footing loaded by airblast overpressure produced by detonation of a nuclear weapon was assumed for design of load pulses on nine model footings used: footing widths of 4.5, 6.0, and 7.5 in. and depth-of-burial to footing width ratios of 0, 0.5, and 1.0; each is a model of a 24-in. square footing in the prototype. The principles of similitude were used to scale length, force, and time in the models. The models were placed in mobile test bins of uniform, fine, dry sand (90 percent relative density) and subjected to dynamic and static loading, producing displacements of not more than one-fourth of footing width.

Nondimensional load-displacement relations dependent only on depth-of-burial ratio were developed relating maximum displacement to peak dynamic load, footing width, and soil shear strength gradient. The relations were normalized by strength and stiffness parameters determined by static tests and reduced to a unique empirical relation valid for dynamic loads up to 1.5 times the static bearing capacity of the footing. Although maximum displacement was apparently unaffected, the response time was distorted because structural mass could not be scaled in the loading system. However, by applying a simple distortion factor, time of maximum displacement was nondimensionally related to peak dynamic load, pulse duration, footing width, soil shear strength, gradient and mass density, structural mass, and acceleration of gravity and was normalized into unique empirical relations by stiffness and strength parameters from static tests, valid for up to 0.8 times the static bearing capacity.

When the dynamic response of the footings in the form of reaction-displacement curves was compared with static response, an increase in initial stiffness and ultimate strength was observed for dynamic loading. However, these dynamic increases were greatest when the static shear strength was lowest, i.e. footings on the surface, and were least for footings buried at a depth equal to its width where the static overburden produced a substantial increase in shear strength. These observations tend to indicate that the apparent strain rate effects were the result of transitory shear strength increases resulting from effective stress increases hypothetically explained as either inertial stresses or pore pressure

reductions (or both) associated with dilatant behavior of dense sands upon shearing. As a consequence, these dynamic increases cannot be reliably utilized in the design of footings for maximum dynamic settlement but must be considered in developing appropriate dynamic foundation resistance functions for use in analytical schemes involving soil-structure interaction as the temporary increases in strength and stiffness of the foundation influence structural response. A trial dynamic resistance function was developed and found to reasonably represent the footing reaction in some cases. In the trial resistance function, dynamic stiffness and strength were related to static strength and applied load parameters whose numerical values can be ascertained from simple tests and design information.

INTRODUCTION

Background

Need for Study

The role of underground protective structures in modern warfare is to provide a survival capability for personnel and equipment in the event of nuclear attack. The response of the foundation of these structures under blast loadings produced by nuclear detonations is critical to the survival of the structure because of its influence on loading of the structure, shock isolation systems, and connections. Conventional approaches to the problem of foundation design based on bearing capacity and settlement tolerances dictated by tolerable structural deformations are no longer applicable since the response of foundations of a protective structure is integrally related to the response of the entire structure. Optimum design must be based on structural behavior of all components, including the foundation, which allow deformations that approach a point of significant interference with the structure's mission at the design overpressure. Thus, definition of the motions of the foundation relative to the free-field in terms of soil properties and structural and loading parameters is required; specifically, load-displacement relations for a range of loads, pulse duration, and soil types.

The conduct of field tests on full-scale structures subjected to actual nuclear blast is the most desirable method of ascertaining the structural response characteristics. However, restrictions on atmospheric testing of nuclear devices by the 1963 Nuclear Test Ban Treaty prohibit such tests, and the researcher must devise other means of developing the information essential for adequate design of protective structures. The response of foundations is recognized to be an exceedingly complex phenomenon and can be treated theoretically only in grossly oversimplified cases. Experimental studies on reduced-scale structure-soil systems using loading devices to simulate nuclear blast loading coupled with adequate modeling techniques offer a strong hope for accomplishment of the specified objectives in spite of field test limitations. Properly scaled tests can define

behavioral phenomena and can indicate the effect of variation of significant parameters.

State-of-the-Art Evaluation

Historically, prior to World War II, very little interest was generated in behavior under nonstatic loading other than settlement of machinery foundations under low amplitude, steady-state vibration. Since 1945, the threat of tremendous energy releases capable of producing high-intensity, short-duration loadings over large areas of the ground surface has led to the development of hardened or blast-resistant construction, both underground and aboveground. In the following paragraphs, selected references relative to theoretical, analytical, and experimental treatments of dynamic behavior of foundations of protective structure and the application of similitude to soil-structure systems are cited, but do not necessarily constitute a complete review of all the available literature in the field of soil dynamics.

Some efforts were made to define dynamic properties of soil, but very little attention had been directed toward the specific problem of footing response prior to 1959 as evidenced by a literature search by Khachaturian (1959). Wallace (1961) and Triandafilidis (1961) extended two-dimensional static-bearing-capacity theories to account for the inertial resistance of the soil which was assumed to move as a rigid body within the bounds of the failure or shear surfaces.

At the University of Illinois, Fisher (1962) conducted small-scale tests on square footings on sand and Johnson and Ireland (1963) conducted tests on square and rectangular footings on clay. Selig and McKee (1961) conducted a number of tests on small footings on sand. Sloan (1962) reported the characteristics of a dynamic loading machine at the U. S. Army Engineer Waterways Experiment Station (WES) and the results of preliminary tests on small-scale footings on sand and clay; Poplin (1965a) reported the results of dynamic tests on square, round, and rectangular small-scale plates of equal area on dense sand. From small-scale footing tests on clay, Jackson and Hadala (1964) and Hadala (1965) demonstrated the feasibility of the use of similitude and developed load-displacement curves in terms of soil, footing, and load parameters for a cohesive soil. These

studies indicated that at equal displacements, dynamic resistance was from 1.5 to 1.9 times greater than static resistance for identical test conditions in cohesive soil. Carroll (1963) used the data from Jackson and Hadala (1964) and Hadala (1965) along with rapid triaxial and field test results to categorize footing response on the basis of stress wave velocity, load rise-time, and footing width and concluded that inertial stresses were of only minor significance in the response of footing in most practical cases. Cunny and Strohm (1963) reported the results of field tests in Nevada during 1962 on spread footings of shallow-buried structures and the response of some of these footings was successfully modeled at a reduced scale in laboratory tests by Hadala and Jackson (1967). At the U. S. Naval Civil Engineering Laboratory, 15-in.-diam plates on sand were tested without overburden (White, 1964a) and with static surface pressures equivalent to overburden up to 15 diameters (White, 1964b), and a significant increase in stiffness with overburden up to 6 diameters was found. Heller (1964) surveyed the available experimental data in 1963 and proposed a failure mode for impact-loaded footings in sand which accounted for lateral inertial resistance of the soil.

As evidenced by the titles of referenced works, considerable effort had been directed toward defining bearing capacity or failure load of the soil for other than static loading. Limit-state theoretical treatments by Wallace (1961) and Triandafilidis (1961) rely heavily upon resistance developed along the same shear surface used to compute static bearing capacity in order to compute time-dependent motion. However, experimental studies with sand have failed to verify the existence of comparable shear surface under dynamic loads except for long-duration loading (Poplin, 1965a), large settlements, or repeated loading (Fisher, 1962; Selig and McKee, 1961). Similarly, tests on clay do not appear to justify the use of theoretical procedures based on static bearing capacity (Johnson and Ireland, 1963; Jackson and Hadala, 1964) for prediction of displacement. In fact, the available test data do not indicate the existence of a well-defined dynamic bearing capacity under dynamic loading. Furthermore, most designs for dynamic conditions are based on a tolerable response (i.e., tolerable displacement) criterion rather than an allowable percentage of

a limit state load. Therefore, the footing motions under a given loading are needed for design. These motions cannot be obtained from limit state theories (Wallace, 1961; Triandafilidis, 1961), but can be determined from dynamic load-displacement relations from properly scaled experimental models.

The principles of similitude and dimensional analysis have only recently been applied in the areas of soil mechanics. Taylor (1948) utilized dimensional analysis to evaluate size effects on footing response and Lundgren (1957) cites extensive usage of dimensional analysis of problems relative to foundations on sand in Denmark since 1950. However, significant utilization by others was not noted until almost a decade later. Jackson and Hadala (1964) showed that maximum displacement of a footing under dynamic loading could be modeled, although some aspects of the model were not properly scaled. Similitude theory has been applied to soil-vehicle systems by Dickson and Yong (1963) and Freitag (1965). Murphy and Young (1962), Murphy et al. (1963), Murphy et al. (1965), and Tener (1964) conducted tests on scaled models of structures of various configurations buried within several soil types but primarily in sand and utilized dimensional analysis as a major aspect of the investigation. These studies of buried structures subjected to dynamically applied surface loading were based on two assumptions:

1. Soil properties could be described by parameters having the same units as pressure.
2. Effect of gravity was negligible.

The first assumption requires unity pressure scaling which restricts the investigation to the same soil in model and prototype and seriously limits the range of length ratios that may be investigated. Also, distortion of gravity (and therefore, gravity-induced stresses) may lead to serious errors because soil stress-deformation and strength properties are often dependent on the state of stress.

At the Naval Civil Engineering Laboratory, experimental studies of thin-walled, footing-supported arches in sand by Allgood et al. (1963) and Gill and Allgood (1964) verified the importance of footings in the overall performance of the structure, particularly in the development of arching

within the soil to partially alleviate loading in the structure. A theory for predicting body motions of a footing of a buried arch was developed by Allgood and DaDeppo (1963) and checked against performance of model arches in high-explosive field tests during Operation Snowball reported by Allgood and Seabold (1965). Complete evaluation of performance was hampered by damage to the models by crater ejecta and comparisons were inconclusive, but it was concluded that modifications of the theory are needed to account for dynamic arching, displacement, and footing load-displacement relations. Sager (1965) reported results of tests on stiff concrete arches during Operation Snowball but crater ejecta also obscured the behavior under the blast loading.

A concise evaluation of the state-of-the-art as of 1965 for design and analysis of footings for protective structures was prepared by Whitman and Luscher (1965). The details of most of the previously cited theoretical and experimental studies are tabulated in this reference. The uncertainties relative to time-dependent load-displacement relations for footings are cited as one of the two major drawbacks in footing design; the other factor is the lack of buried structure footing data. Investigation of the effect of duration of load on peak load-peak displacement relations and tests on models of completely buried structures are recommended as specific needs for future research.

Interpretation of the results of experimental investigation of footing response is hampered by the lack of reliable theories and the random nature of most experimental data. Many theories are available to predict static bearing capacity or limiting load, but even these can yield widely varying results. When ultimate bearing capacity calculated by five well-known theories and experimental results for eight different test conditions were compared by Milovic (1965), it was found that high and low values differed by as much as a factor of two. Theories for predicting settlements of a footing are practically nonexistent due in part to the complex boundary conditions in localized loading, but primarily due to the inability to synthesize the actual behavior of a soil medium with an idealized material. The effects of footing dimensions and depth of burial on settlements of footings in sand are generally understood qualitatively, but a literature

survey of small-scale footing studies (static loading only) by Roberts (1961) showed a wide range of published values. Terzaghi (1955) indicated that theories of subgrade reaction can be used to compute the stresses and bending moments in footings loaded to less than one-half of the static ultimate bearing capacity but should not be used to estimate settlements.

In addition to the lack of workable theories, the many factors that influence footing response introduce inherent experimental errors into test results. Repetition of tests to establish reliability of the data by statistical procedures is not usually feasible. Considerable skill is required to conduct meaningful experimental studies of footing response on sand (Lundgren, 1957). However, when properly used, the technique of modeling and the principles of similitude can greatly enhance interpretation of experimental data. Dimensional analysis can indicate the possible significant variables without knowing the functional relations. The formation of dimensionless terms from the variables permits evaluation of the results of a group of similar tests on a statistical basis.

In many of the cited modeling studies on buried structures, the conditions that either pressure or soil density or both must be scaled at unity impose serious limitation on the range of pressures that can be tested by various laboratory devices. Also, applicability to other soil conditions is particularly restricted by these conditions. These conditions generally result in a distortion of gravitational force which may be of considerable significance in foundations on granular soil. Development of techniques to scale pressures and soil properties would greatly enhance the general application of modeling of foundation response.

Purpose of Study

The purpose of this study was to investigate the applicability of the principles of similitude to the response of foundations on sand and to develop techniques for modeling the response of dynamically loaded footings on sand. The investigation of nonunity scaling of pressure was of particular interest and the development of dimensionless relations between displacement, load, and time for shallow-buried footings in sand was a specific

objective. The effect of width of footings and depth of burial was to be studied.

Scope of Study

To design the experiments for the model study to be within the range of practical applications, a hypothetical prototype situation was assumed. An interior footing, 2 by 2 ft, and appurtenances within a shallow-buried structure, were used as a prototype of small-scale models in laboratory tests. The structure was considered to have been loaded by the overpressure wave produced by a nuclear device of 20-kt yield detonated at 1700 ft above ground zero. The distance between the structure and ground zero was varied to produce selected overpressure-time pulses, which ranged from 1.5-12.5 psi in peak overpressure, with corresponding pulse durations ranging from 1170-680 msec. The time-varying load due to the overpressure was transmitted through the shallow soil cover to the structure's roof and on through a column to the footing to produce a concentric footing load. The configuration of the structure did not permit the overpressure to load the soil adjacent to the footing.

The model testing system consisted of a dynamic loading machine, small-scale footings, and prepared soil specimens. The gas-operated loading machine was capable of applying loads with control of peak load and pulse duration. The soil specimens of dry uniform sand were prepared at 90 percent relative density in mobile metal test bins or carts.

Dimensional analysis of the variables considered to be significant to footing response indicated that for a length scale of n (ratio of length in the prototype to length in the model),* forces scaled by n^3 and time scaled by $\sqrt{n}$ when the soil properties of penetration resistance gradient, i.e., shear strength index, and density were scaled at unity. A distortion of the structural mass was introduced as this parameter could not readily be scaled.

A total of nine models were used in the model study with one static

---

* Symbols are defined when introduced and in Notation on pages ix and x.

and one to six dynamic tests on each model; footing widths were 4.5, 6.0, and 7.5 in. (n = 5.33, 4.00, and 3.20) and depth-of-burial to footing width ratios were 0, 0.5, and 1.0. A range of loads and pulse duration was selected for each model to scale a particular prototype load. The load pulses were selected so as not to exceed an upper limit on displacement of one-fourth of the footing width. This limit was selected because it was believed tolerable footing displacements relative to the free-field would be less than this value. The peak load on the models ranged from 0.4-5.4 kips with corresponding scaled pulse durations from 300-650 msec. Static tests were conducted on each model to determine strength and stiffness characteristics in the absence of dynamic loading.

A total of 23 additional tests were conducted to evaluate the influence of the proximity of specimen boundaries and the spacing between tests. The result of this evaluation showed that the boundaries and spacing used in the model study did not significantly affect footing response.

The data from static load tests were examined in nondimensional form to determine appropriate strength and stiffness parameters and a unique static load-displacement curve was developed for all models. Peak dynamic load, maximum displacement, and time of maximum displacement for all dynamic tests were examined and empirical nondimensional relations were developed. Dynamic footing reaction-displacement relations in nondimensional form were examined and compared with static response to evaluate the effect of footing width and depth of burial on dynamic response.

SIMILITUDE CONSIDERATIONS

Prototype System

A prototype system consisting of a particular structure and weapon was assumed to aid in the selection of physical values for the laboratory model study within the range of practical significance. The assumed prototype system generally conformed to the structure and weapon used in a previous model study by Jackson and Hadala (1964) of dynamic footing response with minor modifications to account for cohesionless soil and shallow-buried footings. Because full-scale testing is not anticipated in the foreseeable future, verification of the proposed scaling laws cannot be accomplished by tests on the prototype. Instead, the scaling laws were verified by comparing test results from a range of model sizes.

The loading on the structure was assumed to be produced by the airblast wave from a nuclear weapon with a yield of 20 kt detonated at 1700 ft above ground zero. Current nuclear weapons effects technology (Glasstone, 1962) was utilized to define the blast loading arriving at the structure. The procedures used by Hadala and Jackson (1967) to design model study experiments for a field test structure similar to the assumed prototype in this study were used as a basis for scaling live loads on the models. The detailed procedures applicable to this study are presented in a supplementary report (Poplin, 1968).*

Model System

The system for modeling the response of the proposed prototype was composed of a dynamic loading device, small-scale footing plates, and soil specimens prepared in mobile bins or carts. The function of the model system was to adequately replicate the equivalent prototype system so that when subjected to properly scaled loading, a scaled response ensued.

---

* A supplementary report, Appendixes A through J, was published in a limited number and is available for loan purposes from the Research Center Library, U. S. Army Engineer Waterways Experiment Station, Vicksburg, Miss.

Features of Loading System

The loading system for the model study consisted of a structural mass called a load column which was restrained to move only in a vertical direction and was loaded by gas pressure. The model load column was in fact the piston of the dynamic loading machine. Reaction at the model footing R(t) was measured directly by a load cell between the load column and the footing. Acceleration of the load column was measured. The column input load analogous to the live load on the prototype was back-figured from the footing load, column mass, and acceleration. The load column and its attached accessories rested firmly on the upper surface of footing plate, and motion of the entire assembly during loading could be considered as rigid body motion. This motion was measured by potentiometers attached to the footings. The intricate details of the nature and interactions of all the forces prevailing within the loading machine during the test cycles were presented and discussed by Jackson and Hadala (1964).

The loading device had a maximum load capacity of 50 kips and could produce pulse durations as short as 30 msec. However, in the interest of safety and reproducible load pulse, operations were limited to peak loads between 0.4 and 10 kips and pulse durations greater than 180 msec.

The greatest disadvantage encountered in the use of the loading device for a model study was the lack of a capability for scaling the mass of the load column analogous to the structural mass of the prototype. The load column assembly used in the model study weighed about 150 lb. By attaching additional weights the total weight could have been increased by a factor of about two but could not be decreased. It will be shown later that this range was inadequate for true modeling and that distortion of mass scaling had to be introduced into the model study.

Footings and Specimens

The specimens of dry, uniform, fine sand (SP) were prepared in a large mobile cart and footings made of 3/4-in.-thick, square aluminum plates were placed in the specimen at the appropriate level during construction. Three plate widths, 4.5, 6.0, and 7.5 in., were selected for the model study. The smallest size was selected as the minimum width that could be satisfactorily used with the available loading device and the

largest size was deemed to be the upper limit without undesirable boundary effects. The specimens were prepared in a special metal cart 11 ft 10 in. long and 40 in. wide, which had a total depth of 36 in., but the lateral boundaries of the lower 12 in. were sloping. A false-bottom boundary of plywood was placed over dense sand in the lower portion at the 20-in. depth so that the volume of the specimen could be accurately determined. The specimens were carefully prepared using a dry sprinkling procedure to produce a high degree of uniformity and were evaluated by independent density and cone penetration tests.

Length, width, and depth of the specimens and spacing between tests in the specimens represented factors that could significantly affect response of the model footing and thereby result in erroneous conclusions relative to prototype behavior. In a supplemental study, tests that were conducted with the specimen depth and width and the spacing between tests approximately doubled showed no significant effects on the footing response (see Appendix F of supplementary report (Poplin, 1968)).

Application of Similitude to Footing Studies

The principles of similitude and dimensional analysis based on Buckingham's Pi Theorem are presented in textbooks on the subject (Langhaar, 1951; Murphy, 1950). Basic details are condensed and summarized in Appendix A of supplementary report (Poplin, 1968).

The successful application of the principles of similitude to an engineering problem requires an insight into the physical mechanisms governing the phenomenon under study. In a complex problem, several different phenomena may interact in such a manner to prohibit exact modeling of a particular problem, and it becomes necessary to identify and attempt to isolate the controlling phenomena.

Soil Properties

Modeling the behavior of a system involving a soil medium as a component requires a critical quantitative evaluation of appropriate soil properties. Displacement of a footing due to loading produces deformation of the soil medium and the primary mechanism activated is the relative

intergranular motion or shear deformation between soil particles. Thus, a relation between shear stress and shear strain is essential to describe the mechanism. While complete definition is desirable, it is not required for adequate modeling if an index can be devised that is quantitatively related to the prevailing stress-strain relations for model and prototype soils.

The capacity of a sand to resist deformation, called shear strength, is derived from friction and interlock between individual grains. The shear strength of dry sand depends on the prevailing normal stress, as indicated by Coulomb's law or equation (Taylor, 1948):

$$\tau_f = \sigma \tan \phi \ , \qquad (1)$$

where

τ_f = shear strength at failure,
σ = normal stress on the plane of failure,* and
ϕ = angle of internal friction.

The normal stress may be due to an applied surface loading or simply the deadweight surcharge of the soil overburden.

After careful consideration of all possible techniques of evaluating shear strength of sand, the method of cone penetration of the prepared test specimen was selected for use in this study. A 30-deg, 1/2-in.-diam right circular cone was pushed into the soil at a constant rate, and the resulting resistance was observed as a function of depth of penetration. Typical data are shown in Figure 1. Shear strength increased with depth but the rate of shear strength increase with depth, called cone penetration resistance gradient G , was reasonably constant. The usefulness of G for describing soil properties of granular media for vehicle mobility studies in sand has been proven (Freitag, 1965; Green et al., 1964). It was found that:

1. For a uniform soil, G was approximately constant within the layers being investigated.

---

* Shear strength depends on the effective stress on the plane of failure which is the difference between total stress and pore pressure on the plane. With dry sand, no excess pore pressures exist under static loading and the total and effective stresses are equal.

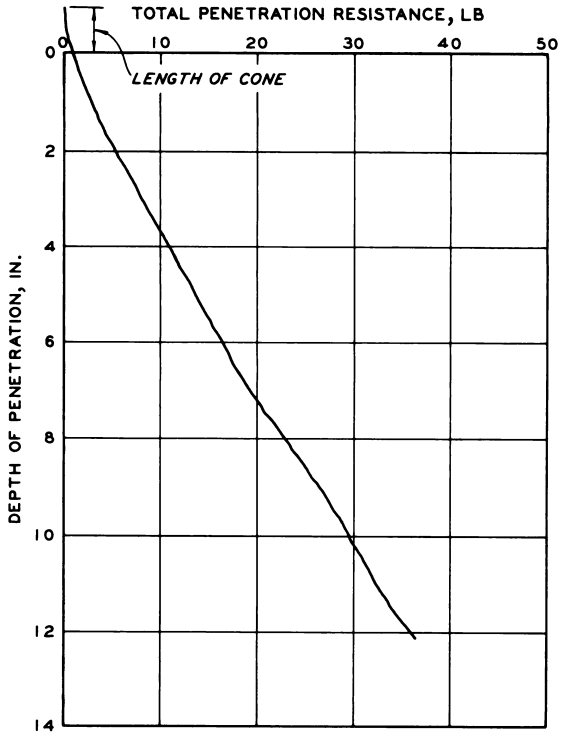

Figure 1. Typical cone penetration test record

2. A direct relation could be developed between G and γ or ϕ.
3. In dry sand, G was relatively insensitive to penetration rate for rates between 1 and 100 in./min. The quantity G was successfully used to nondimensionally relate vehicle performance and soil properties.

The cone penetration gradient computed from the 0- to 6-in. layer in the specimen was selected as the index of static shear strength for the soil medium, i.e., an index property that could be adequately related to a resistance function for the soil-footing system. G has the same qualitative dimensions as γ (FL^{-3}). The choice of this parameter to describe the soil properties is contradictory to the assumptions by Murphy and Young (1962) who assumed that the dominant soil property had dimensions of FL^{-2}.

Resistance Functions

The resistance of the footing and supporting soil was completely defined by the footing load-displacement relation or an R(z) curve for the appropriate time history of loading. In order to ensure that this resistance was correctly modeled, all the factors which influence the footing

load-displacement relation had to be considered in the model: the footing width and depth of burial, the shear strength of the soil, and its stress-strain relation prior to yield.

The geometry of the problem was easily handled by scaling both footing width and burial depth between model and prototype. As indicated earlier, proper scaling of G should be adequate to account for static strength. However, this model study was concerned with dynamic behavior, and the influence of loading rate on strength had to be considered. The experimental evidence available indicates only minor increases, if any, in the strength of dry sands due to high strain rates (Whitman and Healy, 1962). Furthermore for those soils which do appear to have strain rate effects, evidence indicates that these effects are nearly identical at the proposed model and prototype loading rates (Jackson and Hadala, 1964; Tener, 1964). Therefore, correct scaling of static strength was expected to ensure nearly correct scaling of the dynamic strength. No explicit attempts were made in this study to scale the appropriate stress-strain relation for the soil prior to the mobilization of ultimate strength because it was believed that the shear strength of the soil was its dominant property. However, it is known that all those factors which cause an increase in the shear strength of a given sand (in situ density, placement method, and stress history) also increase its stress-strain relation's stiffness. Thus, the behavior prior to the achievement of ultimate strength was not totally ignored.

Another variable not explicitly treated that might be considered to influence the dynamic footing load-displacement relation was stress wave propagation velocity. Based on a criterion developed by Carroll (1963), wave propagation effects were discounted and the stress field under the footing did not essentially deviate from the case of static loading.

Inertial resistance as it affects the footing load-displacement relation is the summation of the vertical inertial forces on individual soil elements. These elemental forces are equal to the product of acceleration and mass. Thus, scaling rules which account for the mass density of the soil ρ and its acceleration including that of gravity g should be adequate to model soil inertial forces.

Pi Terms and Scale Factors

The essential variables considered in the preceding discussion were reduced to 10 variables illustrated in Figure 2 and arranged in a

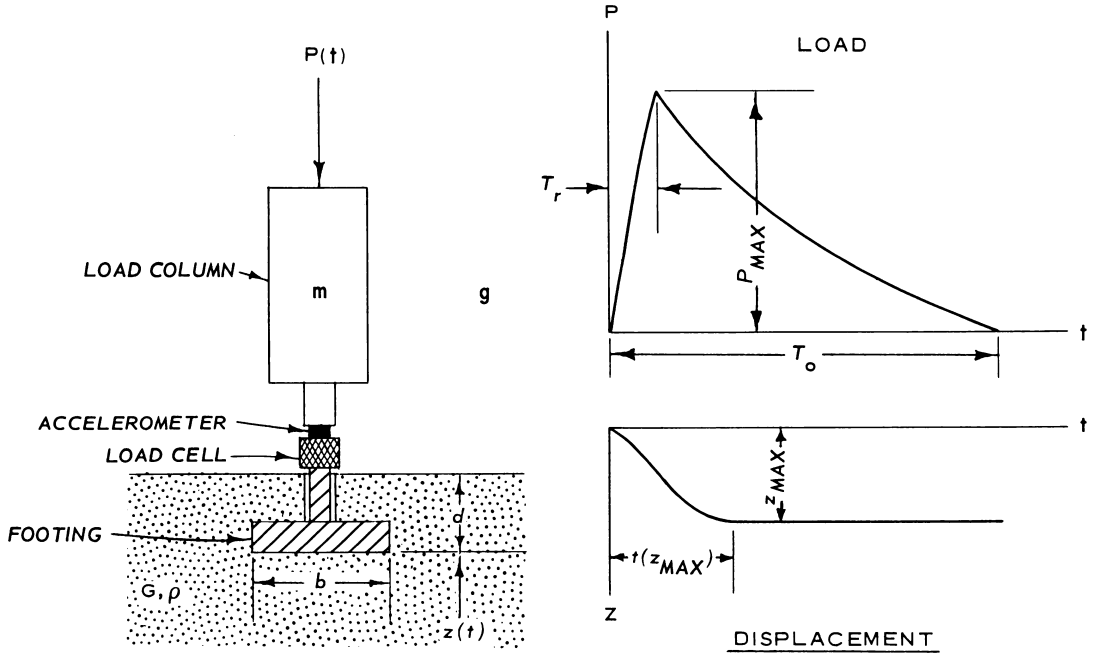

Figure 2. Variables in dynamic tests

functional relation:

$$f(z_{max}, P_{max}, t(z_{max}), b, T_o, d, G, \rho, m, g) = 0, \qquad (2)$$

where

z_{max} = maximum footing displacement under dynamic loading, in.,
P_{max} = peak dynamic load, kips,
$t(z_{max})$ = time of maximum displacement, msec,
b = width of square footing, in.,
T_o = duration of load pulse, msec,
d = depth of burial of footing, in.,
G = average cone penetration resistance gradient (0- to 6-in. depth), psi/in.,
ρ = initial mass density of sand specimen, lb-sec^2/in.^{4},

m = mass of load column (structural mass), lb-sec^2/in., and

g = acceleration of gravity, in./sec^2.

A systematic procedure described in detail by Jackson and Hadala (1964) was used to combine the selected variables into an independent set of non-dimensional pi terms. Of the 10 variables in Equation (2), z_{max} and $t(z_{max})$ were dependent; the remainder were independent in that a change in one variable did not result in a change in any other independent variable. Functional relations between dependent and independent pi terms were developed as follows:

$$\frac{z_{max}}{b} = f_1\left(\frac{P_{max}}{b^3 G}, \frac{d}{b}\right), \tag{3a}$$

$$\frac{t(z_{max})}{T_o} = f_2\left(\frac{P_{max}}{b^3 G}, \frac{d}{b}\right), \tag{3b}$$

$$\frac{P_{max}\left[t(z_{max})\right]^2}{\rho b^4} = f_3\left(\frac{P_{max}}{b^3 G}, \frac{d}{b}\right), \tag{3c}$$

$$\frac{P_{max}\left[t(z_{max})\right]^2}{mb} = f_4\left(\frac{P_{max}}{b^3 G}, \frac{d}{b}\right), \tag{3d}$$

$$\frac{g\left[t(z_{max})\right]^2}{b} = f_5\left(\frac{P_{max}}{b^3 G}, \frac{d}{b}\right). \tag{3e}$$

The test program was designed using the scale factors listed in Table 1 to compute the scale ratio between the independent variables necessary to maintain a unity relation between the pi terms in the model and the

Table 1. Scale factors for model study

Variable	Scale Factor	Numerical Values for Model Footing Widths, in. 4.5	6.0	7.5
Independent				
Footing width, b	n	5.33	4.00	3.20
Pulse duration, T_o	$\sqrt{n}$	2.31	2.00	1.79
Peak dynamic load, P_{max}	n^3	151.70	64.00	32.77
Depth of burial, d	n	5.33	4.00	3.20
Structural mass, m	n^3	151.70	64.00	32.77
Soil mass density, ρ	1	1	1	1
Cone penetration resistance gradient, G	1	1	1	1
Acceleration of gravity, g	1	1	1	1
Dependent				
Maximum footing displacement, z_{max}	n	5.33	4.00	3.20
Time of maximum displacement, $t(z_{max})$	$\sqrt{n}$	2.31	2.00	1.79

prototype. Then, if the tests were conducted as designed, scale factors for the dependent variables as shown in Table 1 should prevail. The scaling rules presented above are comparable to the rules for scaling hydrodynamic phenomena in systems where gravitational acceleration is significant. These rules can be characterized as Froude scaling as the Froude number relates the ratio of inertial force to gravitational force on an element of fluid (Murphy, 1950). The validation and implications of Froude scaling of the response of a soil-footing system will be treated later.

The most serious difficulty arose from the inability to scale the structural mass which should scale as n^3. Circumvention of this difficulty by designing the tests so as to scale mass as unity would tend to make the model study less realistic and perhaps create more serious difficulties. Therefore, the inability to scale this parameter results in a distortion whose effect must be evaluated.

Experimental verification was required to determine the validity of

the scaling rules postulated; this will be presented later. The experimental data could be examined nondimensionally in the form of Equation (3) or all variables could be scaled to the prototype according to the scale factors. In either case, a collapse of the experimental data from the different size models was indicative but not necessarily proof of the validity of postulated scaling relations.

Scaling Rules for Static Tests

Proving the scaling rules developed to be valid for static tests would be quite useful in comparing dynamic response. The dimensional variables for static loading are defined and illustrated in Figure 3 and can be expressed in the functional notation as

$$z_s = f(R_s , b , d , G) . \tag{4}$$

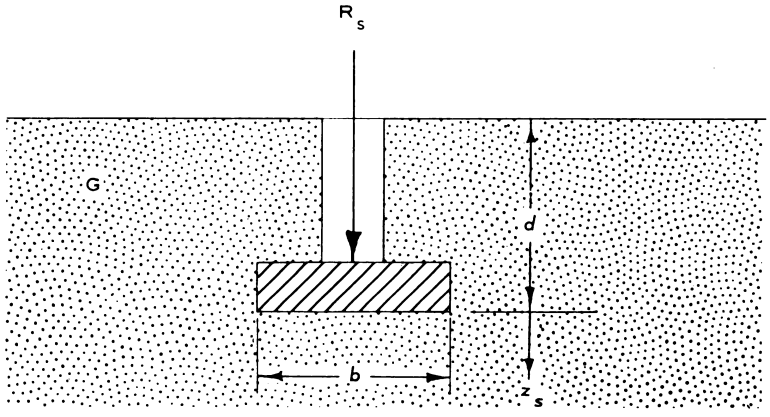

SYMBOL	VARIABLE	DIMENSIONS	TYPE
R_s	STATIC FOOTING REACTION	F	INDEP.
b	WIDTH OF SQUARE FOOTING	L	INDEP.
d	DEPTH OF BURIAL OF FOOTING	L	INDEP.
G	CONE PENETRATION RESISTANCE GRADIENT	FL^{-3}	INDEP.
z_s	VERTICAL DISPLACEMENT OF FOOTING	L	DEP.

Figure 3. Variables in static tests

In this set, z_{max} was replaced by z_s, the static displacement; P_{max} by R_s, the static footing reaction; and the other variables in Equation (2) that involve time were no longer applicable. In the nondimensional form, the static reaction-displacement was:

$$\frac{z_s}{b} = f\left(\frac{R_s}{b^3 G}, \frac{d}{b}\right) . \qquad (5)$$

DESCRIPTION OF MODEL STUDY

Plan of Tests

Nine models were tested using footing widths of 4.5, 6.0, and 7.5 in. and depth-of-burial ratios of 0, 0.5, and 1.0 with from one to six dynamic tests and one static test conducted on each model. A tabulation of the plan of tests is given in Table 2, which shows the numerical design values used to program the load pulses applied to the models.

The individual tests in the model were identified by a specimen or cart number from 36 to 44 and a test number within the specimen from 1 to 7. Six-inch models were prepared in Carts 36, 37, and 38 with depths of burial of 0, 3, and 6 in., respectively. Four dynamic tests at selected scaled prototype overpressure levels p_o and one static test were conducted in each of these carts. Footings 4.5 in. wide were placed in Carts 39 and 40. A very small range between minimum operating load and allowable load was anticipated for the smaller footing so 4.5-in. models with 0- and 2.25-in. depths of burial were placed in the same cart. Two dynamic tests and one static test with footings on the surface were designated Cart 39, and three dynamic tests and one static test at 2.25-in. depth of burial comprised Cart 39A. Six dynamic tests and one static test were conducted on 4.5-in. footing at 4.5-in. depth in Cart 40. Carts 41-44 were prepared with 7.5-in. plates for three dynamic tests and one static test in each cart; surface footings were tested in Cart 41, and buried footings were tested at 3.75 in. in Cart 43 and at 7.5 in. in Carts 42 and 44.

Conduct of Tests

The tests were conducted in accordance with procedural details for static and dynamic footing tests presented in earlier publications (Sloan, 1962; Poplin, 1965a; Jackson and Hadala, 1964; Hadala and Jackson, 1967). Specific details relative to measuring, recording, processing, and interpreting the test data are presented in Appendix B of supplementary report (Poplin, 1968).

Table 2. Plan of tests for model study

Test No.[a]	Location[b] Station	b[c] in.	n	d in.	d/b	p_o psi	P_{max} kips	T_o msec	T_r msec
36-1	2+00	6.0	4.00	0	0	2.5	0.70	525	8
36-2	4+00					4.0	1.12	470	8
36-3	6+00					3.5	0.98	488	8
36-4	8+00					2.0	0.56	550	8
36-5	10+00					Static			
37-1	2+00	6.0	4.00	3.0	0.5	2.5	0.70	525	8
37-2	4+00					3.5	0.98	488	8
37-3	6+00					5.0	1.41	445	8
37-4	8+00					6.5	1.83	415	7
37-5	10+00					Static			
38-1	2+00	6.0	4.00	6.0	1.0	3.5	0.98	488	8
38-2	4+00					11.0	3.09	355	7
38-3	6+00					6.5	1.83	415	7
38-4	8+00					8.5	2.39	385	7
38-5	10+00					Static			
39-1	1+50	4.5	5.33	0	0	Static			
39-2	3+00					4.5	0.54	394	7
39-3	4+50					4.0	0.48	407	7
39A-1	6+00	4.5	5.33	2.25	0.5	4.0	0.54	407	7
39A-2	7+50					3.5	0.42	422	7
39A-3	9+00					8.5	1.01	333	6
39A-4	10+50					Static			
40-1	1+50	4.5	5.33	4.5	1.0	6.0	0.71	368	6
40-2	3+00					10.5	1.25	312	6
40-3	4+50					12.5	1.49	295	6
40-4	6+00					8.5	1.01	333	6
40-5	7+50					9.0	1.07	329	6
40-6	9+00					5.0	0.60	385	6
40-7	10+50					Static			
41-1	2+00	7.5	3.20	0	0	2.0	1.10	615	9
41-2	4+50					3.0	1.65	559	9
41-3	7+00					1.5	0.82	651	9
41-4	9+50					Static			
42-1	2+00	7.5	3.20	7.5	1.0	6.0	3.29	475	8
42-2	4+50					12.0	6.59	386	7
42-3	7+00					3.0	1.65	559	9
42-4	9+50					Static			
43-1	2+00	7.5	3.20	3.75	0.5	5.0	2.75	497	8
43-2	4+50					4.5	2.47	509	8
43-3	7+00					2.0	1.10	615	9
43-4	9+50					Static			
44-1	2+00	7.5	3.20	7.5	1.0	4.5	2.47	509	8
44-2	4+50					9.0	4.94	425	8
44-3	7+00					2.0	1.10	615	9
44-4	9+50					Static			

[a]The following were constants for all tests:
Unit weight, γ = 102.2 pcf (90 percent relative density);
Preload, J = 150 lb (weight of load column, W_c).

[b]Stations are distances from end of cart in feet, plus signs indicate fractions of feet.

[c]See Notation for definition of symbols used in headings.

Of the 35 dynamic tests and 10 static tests shown in the plan of tests in Table 2, all static tests and 31 dynamic tests yielded interpretable data. No record was obtained in Test 39-2 when the loading machine prematurely activated before the recorder started. During Test 39A-1, the lower portion of the load column struck one of the potentiometer upper support beams, invalidating any data after the point of contact. An apparent equipment malfunction during Test 42-2 produced both excessive preload and applied load; as a result, the footing displaced almost 3 in. and exceeded the linearity range of the galvanometers used to sense displacement signals. An electrical cable failure during Test 43-1 resulted in a loss of the load column accelerometer signal, and as a consequence, the applied load could not be computed.

The loss of four test records was unfortunate but did not seriously affect the overall test program as the loading schedule was flexible and adjustments were made in remaining tests to bridge these gaps. The loss of Test 42-2 left only two tests for 7.5-in. footings at 7.5 in., considered to be the most critical condition relative to boundaries of all the models, so Cart 44 was prepared and tested to increase the volume of data for that model.

Presentation of Test Data

The experimental test data for the model study are presented in detail in Appendix C of supplementary report (Poplin, 1968). These data include specimen evaluation test results, reduced oscillograms of load, displacement and acceleration for dynamic tests, and reaction-displacement curves for both dynamic and static tests. Also, procedures for consistent interpretation of the oscillograms to determine numerical values of the significant parameter are outlined and comparisons of the actual and design load pulses are made. The numerical tabulations of the test data are also presented. These data have been summarized in this report and serve as a basis for the analysis to follow.

Control of Independent Variables

In examination, interpretation, and evaluation of the experimental

data, it was noted that some of the design conditions were not fully satisfied. Geometric parameters were controlled in the design and fabrication of test equipment, but soil and loading parameters were subject to experimental variations.

Soil Parameters

The data show that average unit weight γ_d of the test specimens varied no more than ± 0.25 pcf from the target γ_d so the design condition for the soil mass density ρ computed as $\frac{\gamma_d}{g}$ was reasonably satisfied. However, shear strength varied considerably for the 10 specimens, as indicated by the cone penetration resistance gradient G which ranged numerically from 11.9-15.4 psi/in. The question arises as to whether these variations are random or an indication of sensitivity of shear strength with minor variations of other properties.

Plantema (1957) showed that the slope of cone penetration resistance versus depth curve, the angle of internal friction ϕ, and dry unit weight γ_d of a granular soil could be fundamentally related. Direct shear tests related γ_d and ϕ as reported in Appendix B of the supplementary report (Poplin, 1968), so a correlation between G and γ_d remained to be developed. For this purpose, the value of G for each test determined by the average of six to eight penetrations was compared with the average posttest unit weight determined by two adjacent box density samples nearest the test area. The values of G and γ_d for 45 tests in the model study are plotted in Figure 4. Although the range of γ_d was only about 1 percent of the average value, it can be seen from the auxiliary scale that relative density varied from 84-90 percent.* Over this range, G varied from 11.5-15.6 psi/in. The group of four data points from Cart 41 at the center top of Figure 4 failed to correlate with the remainder of the data and reexamination of specimen data for Cart 41 failed to disclose a plausible explanation for this deviation. By disregarding these four points, the remaining data points form a definite correlation between G and γ_d. Although unity scaling of G was not accomplished, the correlation of G with γ_d

* The 1 percent range in γ_d includes random scatter inherent in the sampling device.

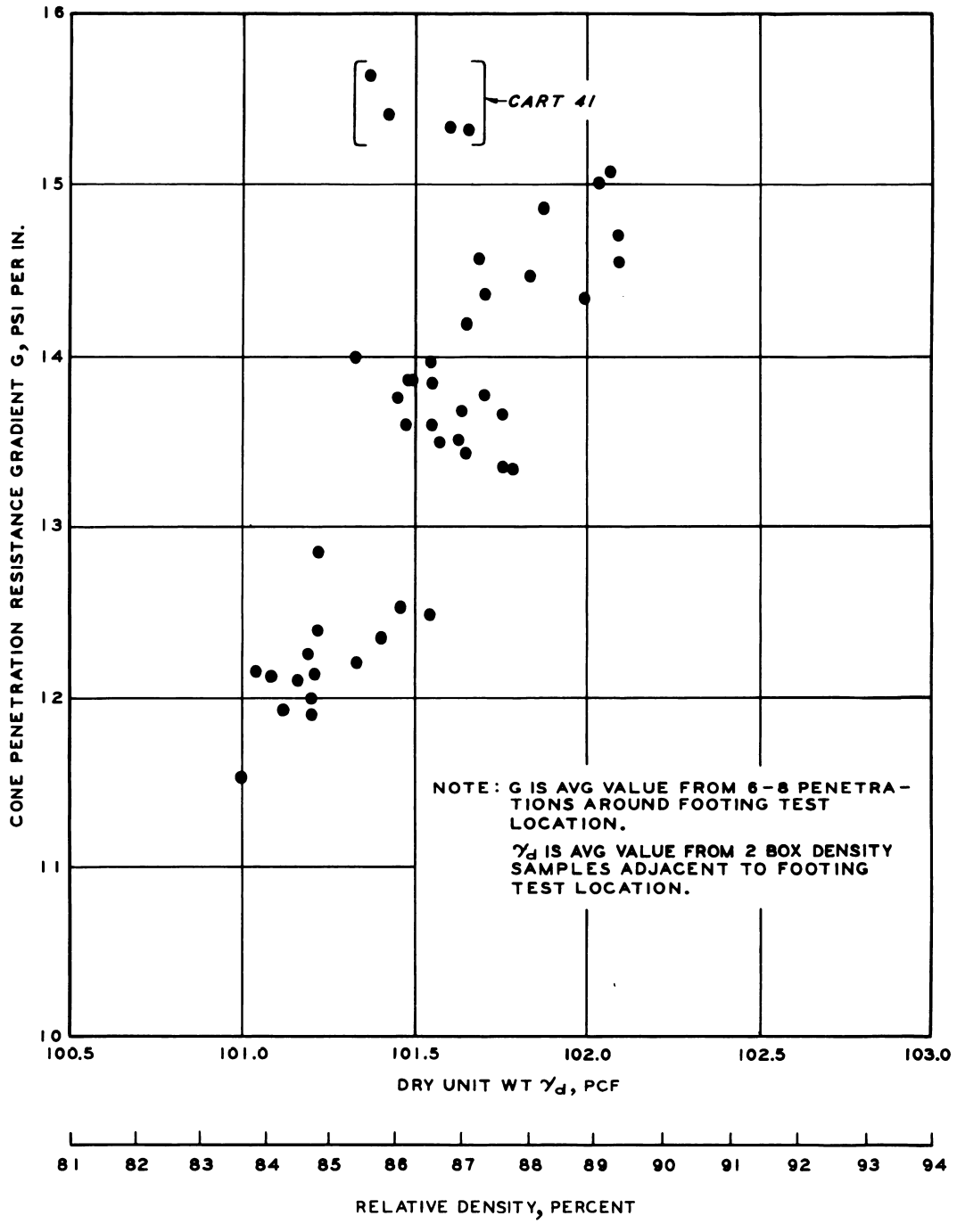

Figure 4. Comparison of cone penetration resistance gradient with unit weight and relative density of specimens

should lead to a useful way of describing and scaling the shear strength of dry granular soil in the study of dynamic and static foundation response.

Load Parameters

The detailed comparison of the actual and design load pulses for each dynamic test revealed no serious discrepancies in scaling the prototype load. In point-by-point comparisons, peak dynamic loads were very close to the target values and variations in actual rise time bracket the design value. Some difficulty in reproducing the exact pulse duration was experienced but the discrepancies were deemed to be inconsequential. The relative time in which the footing was moving compared with the pulse duration showed that these variations had negligible effects. Deviations from the design preload were also found to have no detectable effect on the test results. Thus, the design conditions on these load parameters were effectively satisfied.

ANALYSIS OF STATIC TEST DATA

Validation of Static Scaling Rules

Scaling rules for the response of footings to static loading in Equation (5) indicated that response could be described by:

$$\frac{z_s}{b} = f\left(\frac{R_s}{b^3 G}, \frac{d}{b}\right) . \qquad (5 \text{ bis})$$

To determine the validity of the scaling and the actual functional relation of Equation (5), dimensionless curves were developed from the static test data by plotting $\frac{z_s}{b}$ against $\frac{R_s}{b^3 G}$ with $\frac{d}{b}$ as a third parameter. The resulting nondimensional reaction-displacement curves are shown in Figure 5. The range of these curves forms relatively narrow bands for each depth ratio $\frac{d}{b}$ that are no greater than would be expected from scatter attributable to experimental technique. Tests 42-4 and 44-4 which were tests duplicated on 7.5-in.-square footings differed by as much as the other two curves for 4.5- and 6.0-in.-wide footings at the same depth ratio. Since the range of data for each depth-of-burial to footing width ratio was small, an averaged curve for each depth ratio can be considered a descriptive reaction-displacement relation of Equation (5). The collapse of reaction-displacement curves for different footing sizes at equal depth ratios into unique nondimensional curves is indicative that the postulated scaling rates are valid, at least for the static case. It is important to note that although unity scaling of G was not maintained, modeling was achieved in the sense that these data collapse into a single nondimensional relation for each $\frac{d}{b}$ ratio. This development was interpreted to indicate that the ratio of R_s to G must be scaled as n^3 in order to produce a scaled displacement. The range of G for the investigation was relatively small and final judgment must be reserved until the range can be extended; however, the development presented here appears to indicate that a means of dealing with variable strength conditions in dry, granular soils in model foundation studies has been developed. This aspect will be investigated in future studies.

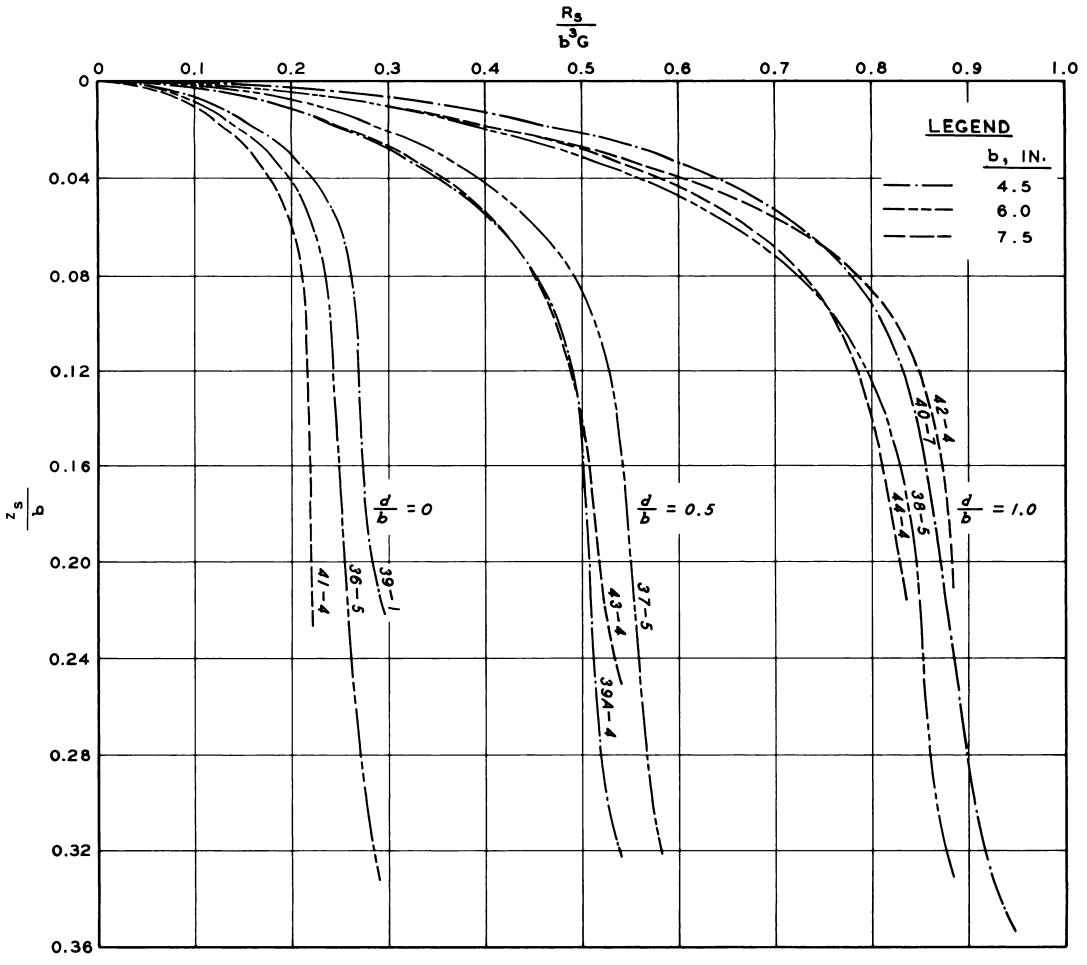

Figure 5. Nondimensional reaction-displacement curves for static tests

Empirical Reaction-Displacement Relations

Curve-Fitting Procedures

An experimentally developed reaction-displacement relation for static loading has considerable utility, but a mathematical expression to approximate the nonlinear function would greatly enhance its usefulness and aid in systematic interpretation of the test data.

While many forms may be used to fit empirical relations (parabolic, exponential, polynomial, trigonometric, etc.), a curve in the form of a rectangular hyperbola was selected to approximate the experimental curves. This choice was made on the basis of simplicity, success in fitting experimental data, physical interpretation of properties of the curve, and the

fact that this type of curve has been utilized by other investigators to describe plate bearing test data and stress-strain relations (Kondner and Krizek, 1962; Murphy, 1965; Carroll, 1963). The nondimensional form of the rectangular hyperbola used to fit the reaction-displacement curves was:

$$\frac{R_s}{b^3 G} = \frac{\frac{z_s}{b}}{A + B\left(\frac{z_s}{b}\right)} , \qquad (6)$$

where

A = the reciprocal of the initial slope of the nondimensional reaction-displacement curve, and

B = the reciprocal of the ultimate value of the parameter $\frac{R_s}{b^3 G}$.

From the experimental curves in Figure 5, average data curves for each depth-of-burial ratio were compiled and the values of A and B for each depth of burial were computed. The values of A and B determined for the three average curves as well as similar values for each of the individual curves in Figure 5 are presented in Table 3.

Table 3. Curve-fitting constants for static reaction-displacement curves

Test No.	b in.	$\frac{d}{b}$	A	B	$\frac{1}{A}$	$\frac{1}{B}$	$\frac{A}{B}$
39-1	4.5	0	0.0493	3.283	20.30	0.3046	0.0150
36-5	6.0	0	0.0547	3.635	18.28	0.2751	0.0151
41-4	7.5	0	0.0535	4.201	18.70	0.2380	0.0127
Averaged curve		0	0.0524	3.672	19.10	0.2723	0.0143
39A-4	4.5	0.5	0.0407	1.732	24.59	0.5775	0.0235
37-5	6.0	0.5	0.0338	1.627	29.61	0.6147	0.0208
43-4	7.5	0.5	0.0421	1.704	23.76	0.5869	0.0247
Averaged curve		0.5	0.0388	1.685	25.80	0.5934	0.0230
40-7	4.5	1.0	0.0197	1.043	50.89	0.9586	0.0188
38-5	6.0	1.0	0.0291	1.024	34.32	0.9763	0.0285
42-4	7.5	1.0	0.0249	0.989	40.21	1.0116	0.0252
44-4	7.5	1.0	0.0246	1.077	40.58	0.9287	0.0223
Averaged curve		1.0	0.0245	1.032	40.77	0.9688	0.0238

Physical Significance of Constants

The constants A and B define a hyperbolic curve and are

independent in that a change in either quantity defines a new curve. Thus, any two of the five quantities involving A and B shown in Table 3 can be used to define a unique relation. The reciprocals of the constants have physical as well as mathematical significance that can be used to describe the behavior of the particular foundation-soil system under study. The dimensionless quantity $\frac{1}{B}$ is the ultimate value $\frac{R_s}{b^3G}$ which occurs at very large displacements and is called the ultimate strength parameter, and $\frac{1}{A}$ is the initial slope or modulus of the nondimensional footing reaction-displacement relation and is called initial stiffness parameter. Although A and B are mathematically independent, physical interdependence exists because both are dependent on the stress-strain characteristics of the soil, and a comparative index of stiffness and strength $\frac{A}{B}$ is called strength-stiffness ratio. The dependence of these quantities on $\frac{d}{b}$ is shown in Figure 6.

In Figure 6a, both individual tests and averaged values of $\frac{1}{B}$ show a distinctly linear variation with $\frac{d}{b}$ which can be reasonably approximated by a straight-line equation

$$\frac{1}{B} = 0.272 \left(1 + 2.6 \frac{d}{b}\right) . \tag{7}$$

The relation for $\frac{1}{A}$ is not as explicit but appears to increase at an increasing rate with depth ratio over the range investigated as shown in Figure 6b. However, the scatter of individual tests increased with depth and no trends relative to footing size were evidenced. When both ultimate strength and initial stiffness were combined into the strength-stiffness ratio $\frac{A}{B}$, it was found to increase at a decreasing rate with depth ratio as shown in Figure 6c. Also, considerable scatter existed at $\frac{d}{b}$ of 1.0 but no trends of possible footing size effects were apparent. Thus, the scatter observed may be attributed to the sensitivity of experimental measurement of stiffness, i.e., the early part of the load displacement relation. This must be considered when applying the constants A and B in other calculations to develop analytical expressions. For purpose of analysis, the values from the averaged curve were found to be adequate to explain fundamental behavior of the soil footing system.

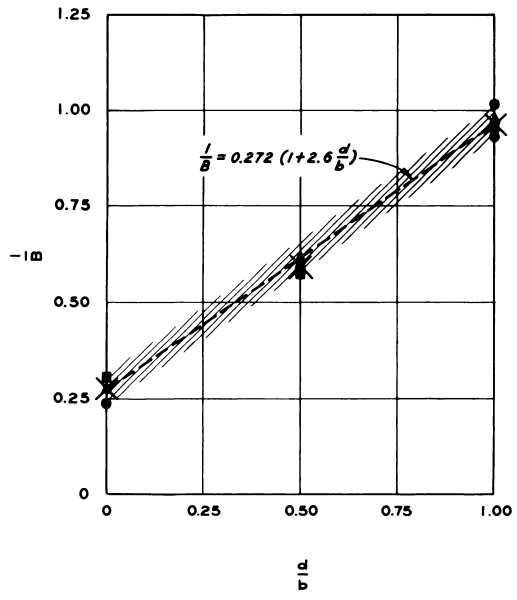

a. ULTIMATE STRENGTH PARAMETER

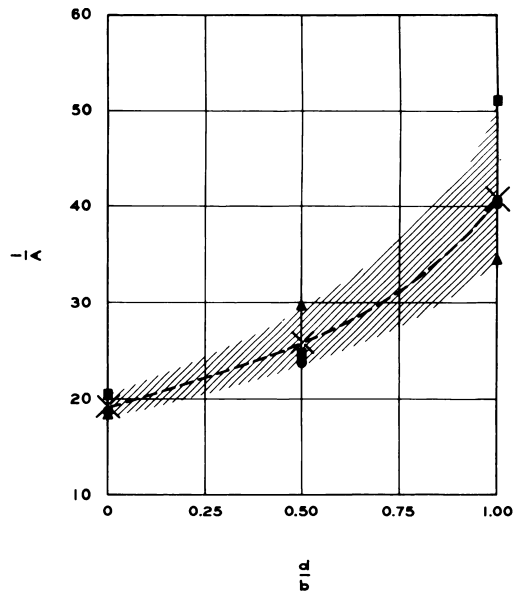

b. INITIAL STIFFNESS PARAMETER

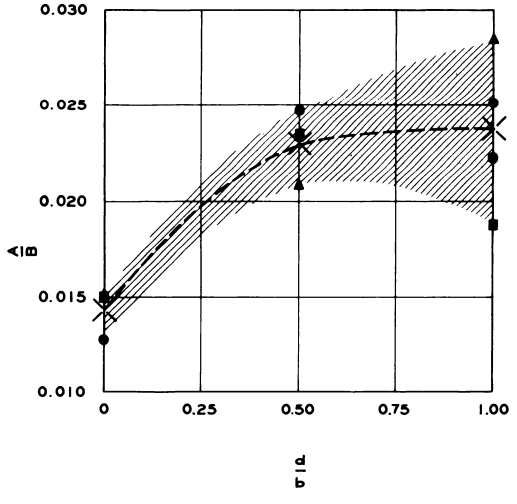

c. STRENGTH - STIFFNESS RATIO

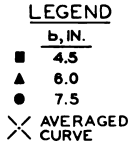

Figure 6. Hyperbolic constants for static reaction-displacement curves versus depth-of-burial ratio

Comparison with Bearing Capacity Theory

The ultimate strength parameter is related to the ultimate static bearing capacity for the system. Theoretical considerations show that the variation in static bearing capacity with depth for a cohesionless soil may be determined by (Taylor, 1948):

$$q_{ud} = q_{uo}\left[1 + C_d\left(\frac{d}{b}\right)\right], \tag{8}$$

where

q_{ud} and q_{uo} = ultimate bearing capacity at a depth and on the surface, respectively, and,

C_d = a depth factor coefficient.

The value of C_d is related to bearing capacity factors, and is a function of the angle of internal friction ϕ for the soil and the prevailing shear failure conditions. For the range of ϕ from 28-38 deg, C_d ranges from 2.2-1.7 for general shear failure and from 3.4-2.4 for local shear failure conditions. When comparison was made with the bearing capacity relations in Figure 7, it found that the ultimate strength parameter curve given in Equation (7) agreed with local shear conditions at ϕ of about 35-36 deg. Visual observations of the surface of the specimen near the footing upon conclusion of the static tests and the shape of reaction-displacement curves tended to indicate that local shear prevailed. Laboratory direct shear tests indicated values of ϕ around 35 deg at 90 percent relative density used in the model study. Thus, the ultimate strength parameter established an upper limit for static bearing capacity, and practical bearing capacities at finite displacements could be defined at an arbitrary proportion of $\frac{1}{B}$. However, refinements of this nature were not required in the model study.

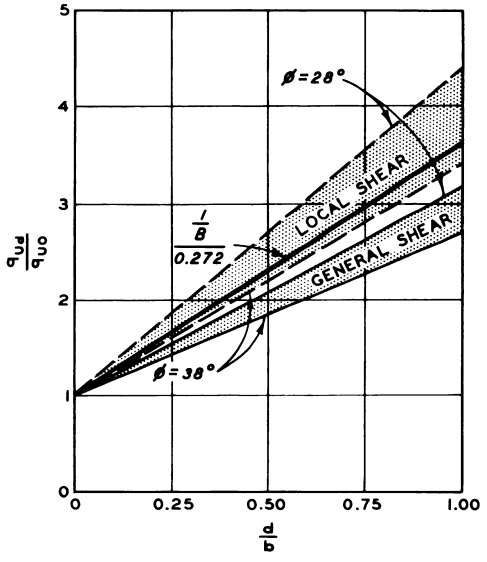

Figure 7. Comparison of ultimate strength parameter with bearing capacity

Normalized Reaction-Displacement Curve

A normalized reaction-displacement relation applicable for depth-of-burial ratios up to 1.0 was developed by dividing Equation (11) by $\frac{1}{B}$ to yield

$$\frac{R_s/b^3G}{1/B} = \frac{z_s/b}{1 + \frac{z_s/b}{A/B}}, \qquad (9)$$

where $\frac{1}{B}$ and $\frac{A}{B}$ become the normalizing factors. To check the validity of the normalization procedure, average curves fitted through the experimental data shown in Figure 5 were reduced by $\frac{1}{B}$ and $\frac{A}{B}$ for the appropriate $\frac{d}{b}$ ratios and plotted in Figure 8. These curves collapse into a unique reaction-displacement curve. Thus, Equation (9) (fitted curve) represents a normalized reaction-displacement relation in terms of dimensionless parameters. Carroll (1963) developed a similar expression for predicting the settlement of a footing on a clay whose stress-strain relations could be described by a two-constant rectangular hyperbola.

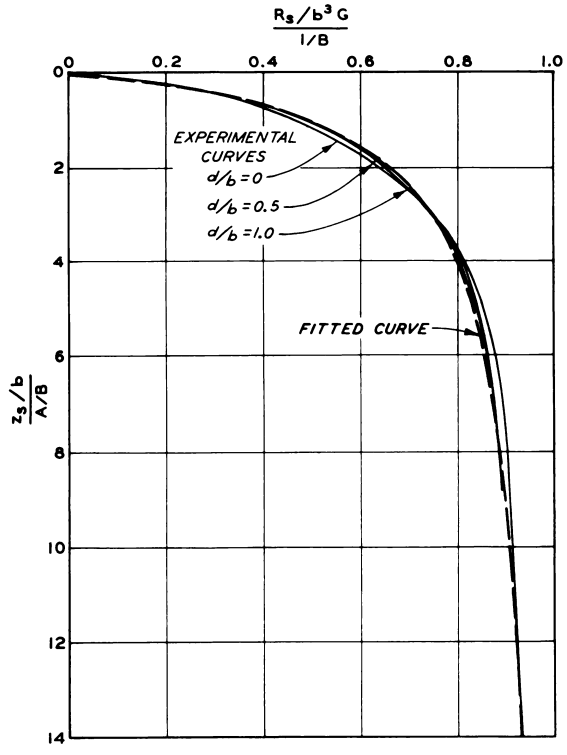

Figure 8. Normalized reaction-displacement curves for static tests

The normalized static load parameter is the ratio of static reaction at any displacement to the ultimate static load occurring at an infinite displacement as defined by the rectangular hyperbola fitting the data. The normalized displacement parameter is the ratio of the displacement an any reaction to a pseudoelastic displacement $\frac{A}{B}$ defined by the intersection of the curves,

$$\frac{R_s}{b^3G} = \frac{1}{A}\left(\frac{z_s}{b}\right) \quad \text{and} \quad \frac{R_s}{b^3G} = \frac{1}{B}.$$

Thus, $\frac{z_s}{b} = \frac{A}{B}$ is a limiting static

displacement if the footing had displaced linearly with a modulus equal to the initial stiffness until reaching the ultimate strength of the footing-soil system.

Nondimensional Dynamic Response Relations

Selection of Variables

The numerical quantities determined in the model study for these 10 parameters listed earlier are tabulated in Table 4. The seven nondimensional pi terms as defined by Equation (3) are presented in Table 5.

Table 4. Dimensional parameters used in analysis

Test No.	z_{max}[a] in.	P_{max} kips	$t(z_{max})$ msec	b in.	T_o msec	d in.	G psi/in.	ρ lb-sec^2/in.^{4}	m lb-sec^2/in.	g in./sec^2
36-1	0.568	0.63	79	6.0	695	0	11.9	153.4×10^{-6}	392.0×10^{-3}	386.4
36-2	1.215	1.02	96		475					
36-3	0.746	0.89	80		635					
36-4	0.293	0.51	72		925					
37-1	0.207	0.64	49	6.0	730	3.0	12.2	153.2×10^{-6}	392.0×10^{-3}	386.4
37-2	0.406	0.98	54		455					
37-3	0.693	1.34	63		615					
37-4	0.866	1.77	67		400					
38-1	0.230	0.98	42	6.0	450	6.0	12.5	153.1×10^{-6}	392.0×10^{-3}	386.4
38-2	1.318	2.98	66		280					
38-3	0.626	1.80	47		320					
38-4	0.914	2.40	55		300					
39-3	0.592	0.49	96	4.5	305	0	14.3	152.9×10^{-6}	379.9×10^{-3}	386.4
39A-2	0.161	0.40	54		530	2.25	14.9			
39A-3	0.742	0.95	71		310					
40-1	0.337	0.69	54	4.5	315	4.5	13.7	153.4×10^{-6}	379.9×10^{-3}	386.4
40-2	0.824	1.20	62		255					
40-3	1.073	1.44	69		255					
40-4	0.440	0.96	53		275					
40-5	0.469	1.02	54		275					
40-6	0.200	0.59	40		450					
41-1	0.369	1.14	47	7.5	640	0	15.4	153.1×10^{-6}	392.0×10^{-3}	386.4
41-2	0.663	1.67	61		570					
41-3	0.161	0.67	41		875					
42-1	0.438	3.17	33	7.5	375	7.5	13.8	152.9×10^{-6}	392.0×10^{-3}	386.4
42-3	0.130	1.45	26		550					
43-2	0.462	2.46	45	7.5	440	3.75	14.4	152.9×10^{-6}	392.0×10^{-3}	386.4
43-3	0.104	0.94	32		665					
44-1	0.332	2.56	33	7.5	400	7.5	13.5	152.9×10^{-6}	392.0×10^{-3}	386.4
44-2	0.956	5.06	58		330					
44-3	0.080	1.16	22		650					

[a] See Notation for definition of symbols in headings.

Table 5. Nondimensional pi terms used in analysis

Test No.	$\frac{P_{max}}{b^3G}$	$\frac{d}{b}$	$\frac{z_{max}}{b}$	$\frac{t(z_{max})^a}{T_o}$	$\frac{P_m[t(z_{max})]^2}{\rho b^4}$	$\frac{P_{max}[t(z_{max})]^2}{mb}$	$\frac{g[t(z_{max})]^2}{b}$
36-1	0.245	0	0.0947	0.114	19.78	1.672	0.402
36-2	0.399		0.2025	0.202	47.28	3.997	0.594
36-3	0.346		0.1243	0.126	28.65	2.422	0.412
36-4	0.198		0.0488	0.078	13.30	1.124	0.334
37-1	0.243	0.5	0.0345	0.067	7.74	0.653	0.155
37-2	0.371		0.0677	0.119	14.39	1.215	0.188
37-3	0.509		0.1155	0.102	26.79	2.261	0.256
37-4	0.672		0.1443	0.168	40.02	3.378	0.289
38-1	0.363	1.0	0.0383	0.093	8.71	0.735	0.114
38-2	1.103		0.2197	0.236	65.42	5.519	0.281
38-3	0.667		0.1043	0.147	20.04	1.691	0.142
38-4	0.889		0.1523	0.183	36.59	3.087	0.195
39-3	0.376	0	0.1316	0.315	72.02	2.641	0.791
39A-2	0.295	0.5	0.0358	0.102	18.60	0.682	0.250
39A-3	0.700		0.1649	0.229	76.38	2.801	0.433
40-1	0.553	1.0	0.0749	0.171	31.99	1.177	0.250
40-2	0.961		0.1831	0.243	73.33	2.698	0.330
40-3	1.154		0.2384	0.271	108.99	4.010	0.409
40-4	0.769		0.0978	0.193	42.87	1.577	0.241
40-5	0.817		0.1042	0.196	47.28	1.740	0.250
40-6	0.472		0.0444	0.089	15.01	0.552	0.137
41-1	0.175	0	0.0492	0.073	5.20	0.857	0.114
41-2	0.257		0.0884	0.117	12.83	2.114	0.192
41-3	0.103		0.0215	0.047	2.32	0.383	0.087
42-1	0.544	1.0	0.0584	0.088	7.14	1.174	0.056
42-3	0.249		0.0173	0.047	2.03	0.333	0.035
43-2	0.405	0.5	0.0616	0.102	10.30	1.694	0.104
43-3	0.155		0.0139	0.048	1.99	0.327	0.053
44-1	0.450	1.0	0.0443	0.083	5.76	0.948	0.056
44-2	0.888		0.1275	0.176	35.18	5.790	0.173
44-3	0.204		0.0106	0.034	1.16	0.191	0.025

[a] T_o is actual pulse duration.

In this set of variables, both z_{max} and $t(z_{max})$ are dependent variables and the remainder are independent. When these variables are combined into seven pi terms, only $\frac{d}{b}$ and $\frac{P_{max}}{b^3G}$ are comprised wholly of independent terms. The term $\frac{d}{b}$ was an arbitrary constant for a given model but $\frac{P_{max}}{b^3G}$ varied from test to test. Thus, unique relations as indicated by Equations (3a)-(3e) should exist between $\frac{P_{max}}{b^3G}$ and pi terms involving dependent variables at the various $\frac{d}{b}$ ratios if the assumed scaling rules are valid.

Peak Dynamic Load-Maximum Displacement

To examine the relation between load and displacement for the pulse type dynamic loads, the dependent pi term $\frac{z_{max}}{b}$ was plotted against $\frac{P_{max}}{b^3G}$ as shown in Figure 9. For each $\frac{d}{b}$ ratio, these data points collapsed into distinct relations with no tendencies toward grouping with respect to footing size. The increase in strength with depth of burial appears to be in approximately the same proportion as observed in static reaction-displacement curves (see Figure 5). The interrelation between static and dynamic response will be investigated further in the search for normalizing factors. The unique relations shown in Figure 9 indicate that maximum displacements were not significantly distorted and the scaling rules used are valid for the model study.

Peak Dynamic Load-Time of Maximum Displacement

The dependent pi terms involving time, $\frac{P_{max}[t(z_{max})]^2}{mb}$, $\frac{P_{max}[t(z_{max})]^2}{\rho b^4}$, $\frac{t(z_{max})}{T_o}$, and $\frac{g[t(z_{max})]^2}{b}$, were plotted against $\frac{P_{max}}{b^3G}$ in Figure 10. In general, these data points only formed unique relations for a particular size model. In Figure 10a, it was noted that for a given value of $\frac{P_{max}}{b^3G}$, $\frac{P_{max}[t(z_{max})]^2}{mb}$ increased with decreasing $\frac{d}{b}$ similar to

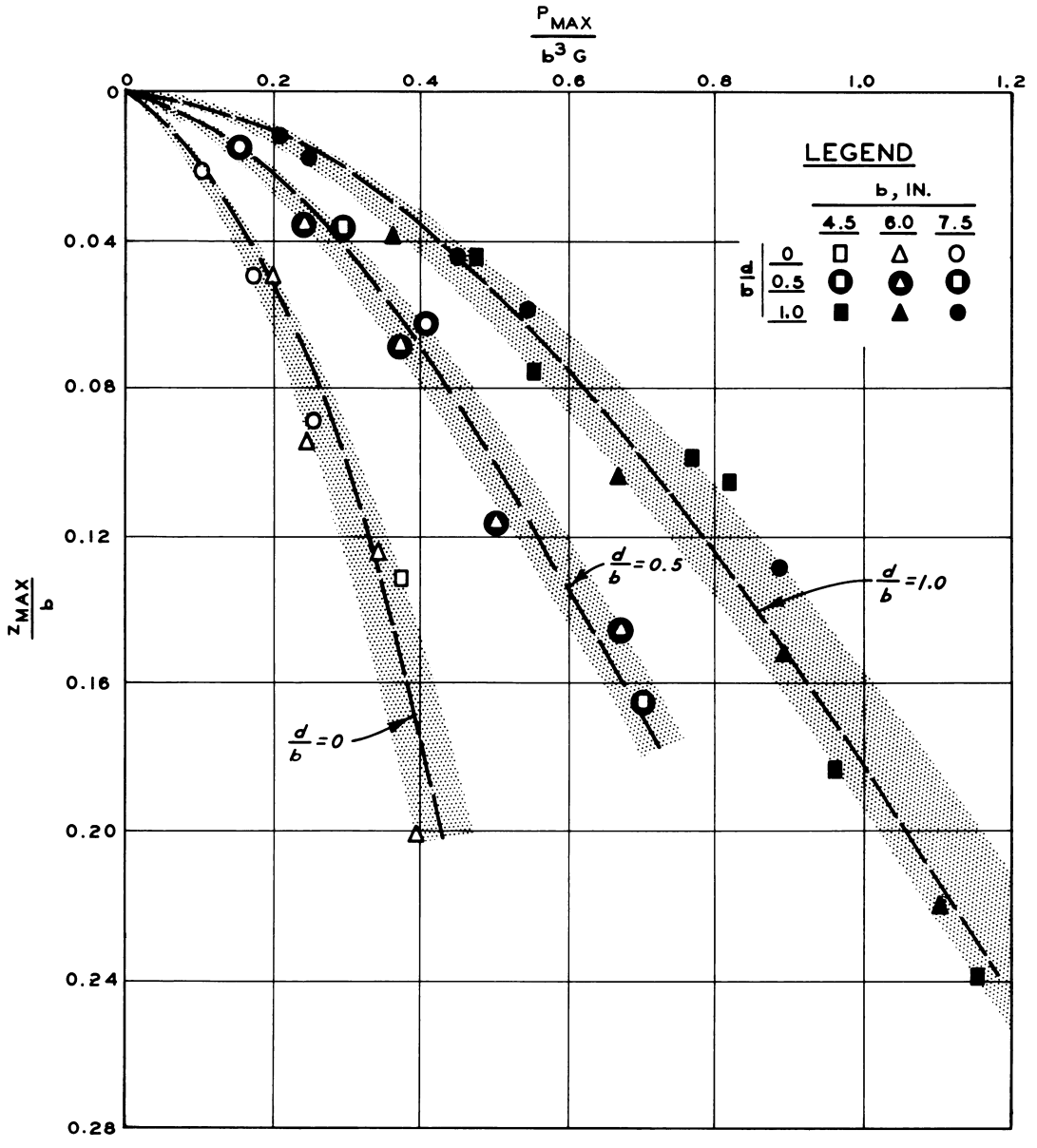

Figure 9. Nondimensional peak dynamic load-maximum displacement relations

the effect observed on $\frac{z_{max}}{b}$. However, for a given $\frac{d}{b}$ and $\frac{P_{max}}{b^3 G}$ this parameter increased with increase in footing width. In plots of the other three dependent pi terms against $\frac{P_{max}}{b^3 G}$ (Figures 10b, c, and d), the

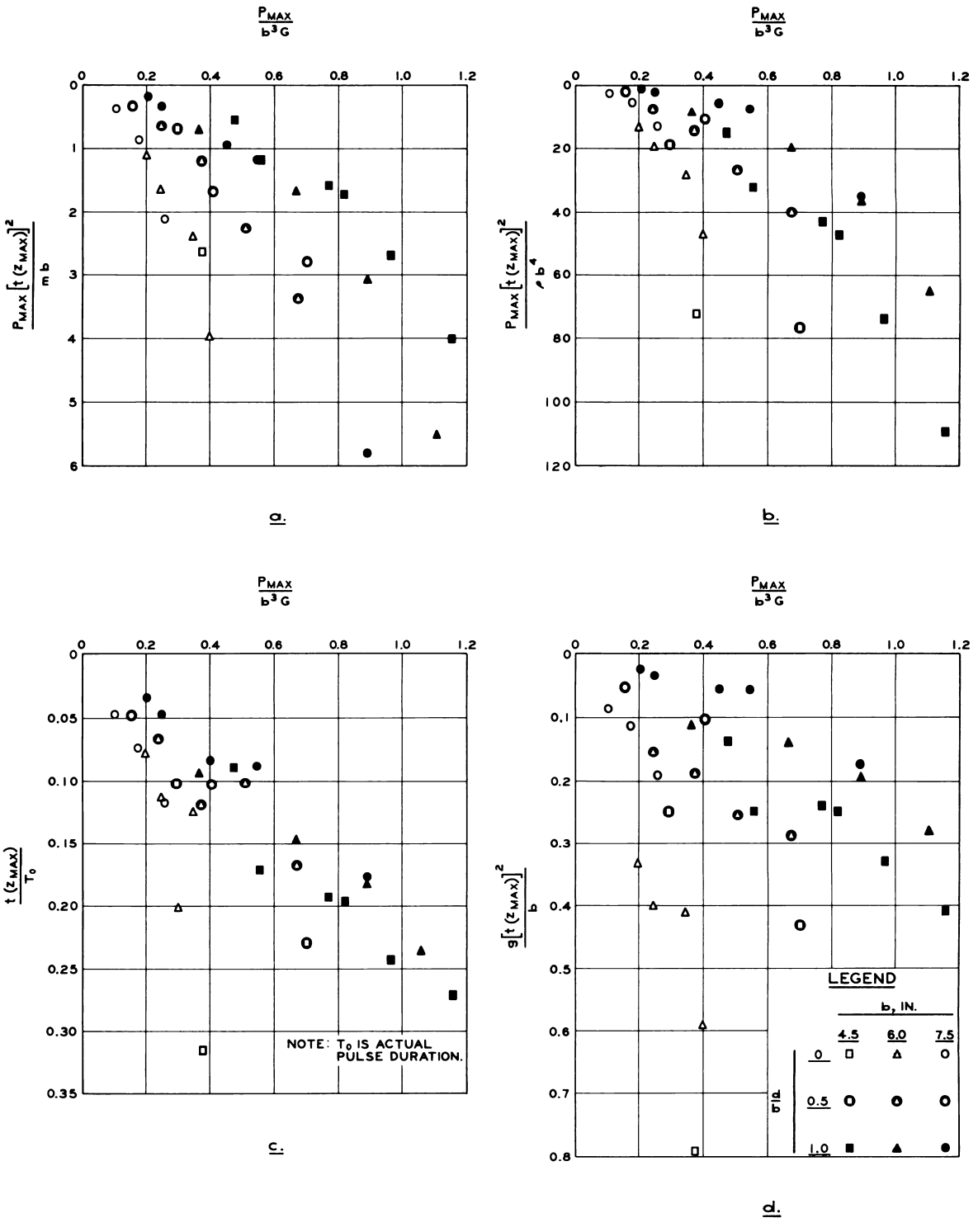

Figure 10. Nondimensional peak dynamic load-time of maximum displacement relations

dependent nondimensional time parameters increased with decreasing $\frac{d}{b}$. At a particular $\frac{d}{b}$ and $\frac{P_{max}}{b^3 G}$, smaller values of $\frac{P_{max}[t(z_{max})]^2}{\rho b^4}$, $\frac{t(z_{max})}{T_o}$, and $\frac{g[t(z_{max})]^2}{b}$ were observed for larger footing widths, the opposite effect to that noted in Figure 10a. The lack of collapse of these data points is indicative of distortion of time scaling incurred by the inability to scale the structural mass. The next step was to conduct a distortion analysis of the test data.

Distortion Analysis

In the development of the model study, consideration was given to designing a distorted model using the compensating distortion factors to adjust for mass distortion. Since satisfaction of all the requirements was not feasible, the independent parameters were not distorted in the design of the tests. However, the test results have indicated distortion of $t(z_{max})$, a dependent variable under consideration and distortion factors were utilized to examine this particular effect.

The pi term $\frac{t(z_{max})}{T_o}$ involves time only and a comparison of this term with $\frac{P_{max}}{b^3 G}$ should nondimensionally relate peak dynamic load and time of maximum displacement. However, the plot of data points for these parameters in Figure 10c are scattered to the extent that only general trends can be detected. In examining the test results, it was noted that the actual pulse duration deviated considerably from the design pulse duration. Since maximum displacement occurred early in the pulse duration, assuming that $t(z_{max})$ is insensitive to minor deviations of T_o is reasonable. Thus, valid comparisons using a dimensionless parameter involving the design pulse duration were made.

A useful technique in dimensional analysis derives from the mathematical condition that a given set of pi terms is independent but not necessarily unique (Murphy, 1950). Therefore, any pi term may be replaced by combination with other dimensionless terms to form a new set of independent

pi terms. Thus, the ratio $\frac{(T_o)_{actual}}{(T_o)_{design}}$ can be combined with $\frac{t(z_{max})}{(T_o)_{actual}}$ to form an alternate pi term $\frac{t(z_{max})}{(T_o)_{design}}$. For purposes of analysis, future references to T_o unless otherwise specified indicate the design pulse duration instead of the actual duration.

To qualitatively assess the effect of mass distortion, the 6-in. models were assumed to be undistorted models. Mass in excess of the properly scaled mass for the 4.5-in. models would be expected to produce a time to maximum displacement greater than predicted by undistorted scaling. Also, insufficient mass in the 7.5-in. model would produce a time to maximum displacement smaller than predicted (Hadala and Jackson, 1967). A trend of this nature was observed in the relations of $\frac{P_{max}}{b^3G}$ and each of the non-dimensional time to maximum displacement parameters shown in Figure 10.

Distortion factors for response time β due to the distortion of structural mass given were 0.7, 1.0, and 1.4 for 4.5-, 6.0-, and 7.5-in.-wide footings, respectively.* Since application of these analytically developed factors would result in adjustments in the time to maximum displacement in the direction required to eliminate the apparent footing size influence in Figure 10, the use of these factors was a logical choice. Therefore, the relations in Figure 10 were adjusted by multiplying $t(z_{max})$ by the appropriate value of β. The numerical values of the pi terms adjusted for mass distortion are listed in Table 6. Unique relations dependent only on $\frac{d}{b}$ ratio resulted from this operation and are shown in Figure 11.

The relation between $\frac{P_{max}}{b^3G}$ and $\frac{\beta t(z_{max})}{T_o}$ (Figure 11a) appears to be almost linear over the range of the data. Deviations from the linear relation were observed at $\frac{d}{b}$ of 1.0 for the highest values of $\frac{P_{max}}{b^3G}$ for both 6- and 7.5-in. footings, which at first appeared to be explainable as

---

* The procedure for computing the distortion factors is presented in Appendix A of supplementary report (Poplin, 1968).

Table 6. Pi terms adjusted for mass distortion

Test No.	$\frac{P_{max}}{b^3 G}$	$\frac{z_{max}}{b}$	$\frac{\beta t(z_{max})}{T_o}$ [a]	$\frac{P_{max}[\beta t(z_{max})]^2}{\rho b^4}$	$\frac{g[\beta t(z_{max})]^2}{b}$	$\frac{P_{max}[t(z_{max})]^3}{mbT_o}$	$\frac{z_{max}}{g[\beta t(z_{max})]^2}$
36-1	0.245	0.0947	0.150	19.78	0.402	0.251	0.236
36-2	0.397	0.2025	0.204	47.28	0.594	0.815	0.341
36-3	0.346	0.1243	0.164	28.65	0.412	0.397	0.302
36-4	0.198	0.0488	0.131	13.30	0.334	0.147	0.146
37-1	0.243	0.0345	0.093	7.74	0.155	0.061	0.223
37-2	0.371	0.0677	0.111	14.39	0.188	0.135	0.360
37-3	0.509	0.1155	0.141	26.79	0.256	0.319	0.451
37-4	0.672	0.1443	0.161	40.02	0.289	0.544	0.499
38-1	0.363	0.0383	0.086	8.71	0.114	0.063	0.336
38-2	1.103	0.2197	0.186	65.42	0.281	1.025	0.782
38-3	0.667	0.1043	0.113	20.04	0.142	0.191	0.735
38-4	0.889	0.1523	0.143	36.59	0.195	0.442	0.781
39-3	0.376	0.1316	0.167	36.01	0.396	0.624	0.332
39A-2	0.295	0.0358	0.091	9.30	0.125	0.088	0.286
39A-3	0.700	0.1649	0.151	38.19	0.216	0.596	0.762
40-1	0.553	0.0749	0.104	16.00	0.125	0.173	0.600
40-2	0.961	0.1831	0.140	36.66	0.165	0.537	1.110
40-3	1.154	0.2384	0.165	54.50	0.204	0.935	1.166
40-4	0.769	0.0978	0.113	21.44	0.120	0.253	0.812
40-5	0.817	0.1042	0.116	23.64	0.125	0.287	0.834
40-6	0.472	0.0444	0.074	7.50	0.068	0.057	0.658
41-1	0.175	0.0492	0.107	10.40	0.228	0.065	0.216
41-2	0.257	0.0884	0.154	25.66	0.384	0.224	0.230
41-3	0.103	0.0215	0.089	4.64	0.164	0.024	0.124
42-1	0.544	0.0584	0.098	14.28	0.112	0.082	0.572
42-3	0.249	0.0173	0.065	4.06	0.070	0.015	0.287
43-2	0.405	0.0616	0.124	20.60	0.208	0.149	0.296
43-3	0.155	0.0139	0.073	3.98	0.106	0.017	0.131
44-1	0.450	0.0443	0.093	11.52	0.112	0.063	0.396
44-2	0.888	0.1275	0.194	70.36	0.346	0.793	0.368
44-3	0.204	0.0106	0.051	2.32	0.050	0.007	0.212

[a] T_o is design pulse duration.

erroneous data. However, examination of the test record for the 6-in. footing in Test 38-2 revealed somewhat nontypical acceleration and displacement histories and similar behavior was noted for the 7.5-in. footing in Test 44-2. In each test, the peak negative acceleration was smaller relative to the peak positive acceleration than in all the other tests

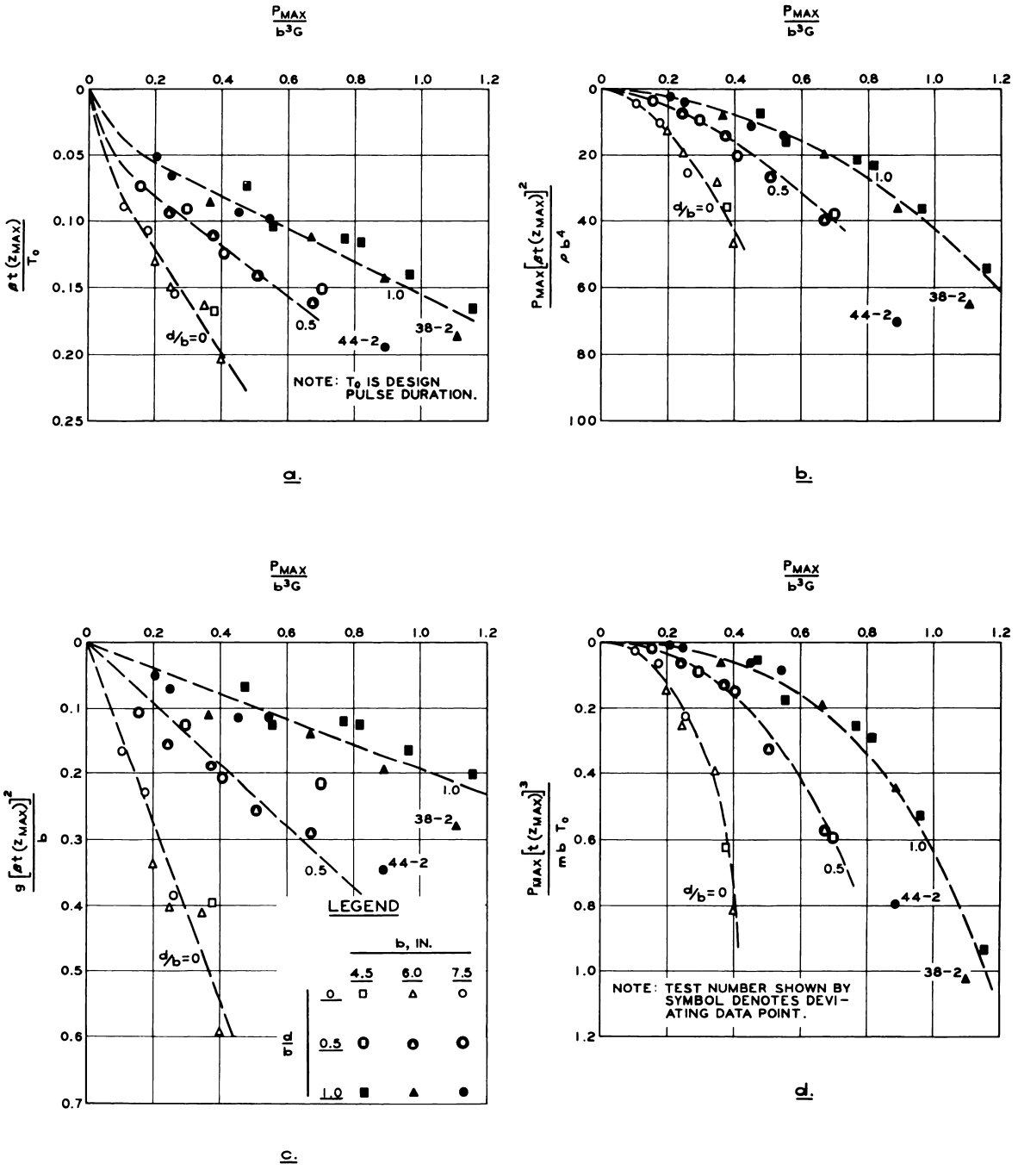

Figure 11. Nondimensional peak dynamic load-time of maximum displacement relations adjusted for mass distortion

which was reflected in a longer time required to bring the footing to rest. The observed quasi-plastic behavior can rationally be explained as a yielding phenomenon within the sand specimen which prolonged the time to maximum displacement but did not significantly increase maximum displacement. Based on this sparse evidence, the threshold to the yielding phenomenon appeared to be dependent on footing size. Application of β to the relation shown in Figure 10b collapsed $\frac{P_{max}[\beta t(z_{max})]^2}{\rho b^4}$ versus $\frac{P_{max}}{b^3 G}$ into distinct relations dependent only on $\frac{d}{b}$ (with the exceptions noted earlier) as shown in Figure 11b. Similarly, $\frac{g[\beta t(z_{max})]^2}{b}$ collapsed into unique relations for each depth ratio as seen in Figure 11c when the time distortion factor was applied to $t(z_{max})$.

The relation between $\frac{P_{max}}{b^3 G}$ and $\frac{P_{max}[t(z_{max})]^2}{mb}$ (Figure 10a) presents a special case since two distorted variables are involved in the dependent parameter. Application of the distortion factor for time β to $t(z_{max})$ alone would further distort the relation, and application of distortion factors for mass and time would have a nullifying effect. However, opposing distortion effects were observed in $\frac{P_{max}[t(z_{max})]^2}{mb}$ and $\frac{t(z_{max})}{T_o}$.* Combining these two pi terms produced a new pi term $\frac{P_{max}[t(z_{max})]^3}{mbT_o}$. When the new pi term was plotted against $\frac{P_{max}}{b^3 G}$ as shown in Figure 11d, unique relations dependent only on $\frac{d}{b}$ evolved. Thus, nondimensional peak dynamic load-time of maximum displacement relations at

---

* The design pulse duration was used, based on considerations previously discussed.

least valid for the model study data were developed without the use of distortion factors.

Normalized Dynamic Response Relations

Nondimensional relations have been established for peak dynamic load-maximum displacement and peak dynamic load-time of maximum displacement that are dependent only on $\frac{d}{b}$ ratios. Differences in response at various depth-of-burial ratios can be directly attributed to differences in stiffness and strength of the soil-footing systems. Reductions of the developed relations into a unique relation irrespective of depth-of-burial ratio would increase the generality of application of test results and indicate possible means of relating the various nondimensional terms in empirical expressions.

Peak Dynamic Load-Maximum Displacement

A possible method of collapsing load-displacement relations was indicated when reaction-displacement curves from the static tests were combined into a single curve. The peak dynamic load-maximum displacement relations were normalized in a similar manner by dividing $\frac{P_{max}}{b^3 G}$ and $\frac{z_{max}}{b}$ by the ultimate strength parameter $\frac{1}{B}$ and strength-stiffness ratio $\frac{A}{B}$, respectively. The normalizing factors $\frac{1}{B}$ and $\frac{A}{B}$ were the same values from the appropriate $\frac{d}{b}$ ratio used to collapse the static reaction-displacement curve in Figure 8. The normalized data points, tabulated in Table 7 and plotted in Figure 12, show that load and displacement were reduced to a unique relation independent of depth of burial. The collapse of the data points was quite satisfactory considering the normalizing factors were experimentally determined from a limited number of observations.

The experimental data in Figure 12 and other normalized data to be presented were fitted by empirical curves, using standard curve-fitting techniques as used by Hadala (1965) to fit similar data. The empirical equations and curves are shown along with the experimental data.

The fact that load-displacement relations for various depths of burial can be reduced to a unique relation represents an important finding

Table 7. Normalized pi terms

Test No.	P_{max}/b^3G 1/B	z_{max}/b A/B	$\beta t(z_{max})^a / T_o$	$P_{max}[\beta t(z_{max})]^2/\rho b^4$ A/B	$P_{max}[t(z_{max})]^3/mbT_o$ A/B
36-1	0.901	6.622	0.150	1383	17.55
36-2	1.459	14.161	0.204	3306	56.99
36-3	1.272	8.692	0.164	2003	27.76
36-4	0.728	3.413	0.131	930	10.28
37-1	0.410	1.500	0.093	337	2.65
37-2	0.626	2.943	0.111	626	5.87
37-3	0.858	5.022	0.141	1165	13.87
37-4	1.133	6.274	0.161	1740	23.65
38-1	0.375	1.609	0.086	366	2.65
38-2	1.138	9.231	0.186	2749	43.07
38-3	0.688	4.382	0.113	842	8.03
38-4	0.917	6.399	0.143	1537	18.57
39-3	1.382	9.203	0.167	2518	43.64
39A-2	0.497	1.557	0.091	405	3.82
39A-3	1.180	7.170	0.151	1660	25.91
40-1	0.571	3.147	0.104	672	7.27
40-2	0.992	7.693	0.140	1540	22.56
40-3	1.191	10.017	0.165	2290	39.29
40-4	0.794	4.109	0.113	900	10.63
40-5	0.843	4.378	0.116	993	12.06
40-6	0.487	1.866	0.074	315	2.39
41-1	0.643	3.441	0.107	728	4.55
41-2	0.945	6.182	0.154	1794	15.66
41-3	0.379	1.503	0.089	324	1.68
42-1	0.561	2.454	0.098	600	3.45
42-3	0.257	0.727	0.065	216	0.63
43-2	0.683	2.678	0.124	896	6.48
43-3	0.261	0.604	0.073	174	0.74
44-1	0.464	1.861	0.093	484	2.65
44-2	0.916	5.357	0.194	2956	33.32
44-3	0.211	0.445	0.054	98	0.29

[a] T_o is design pulse duration.

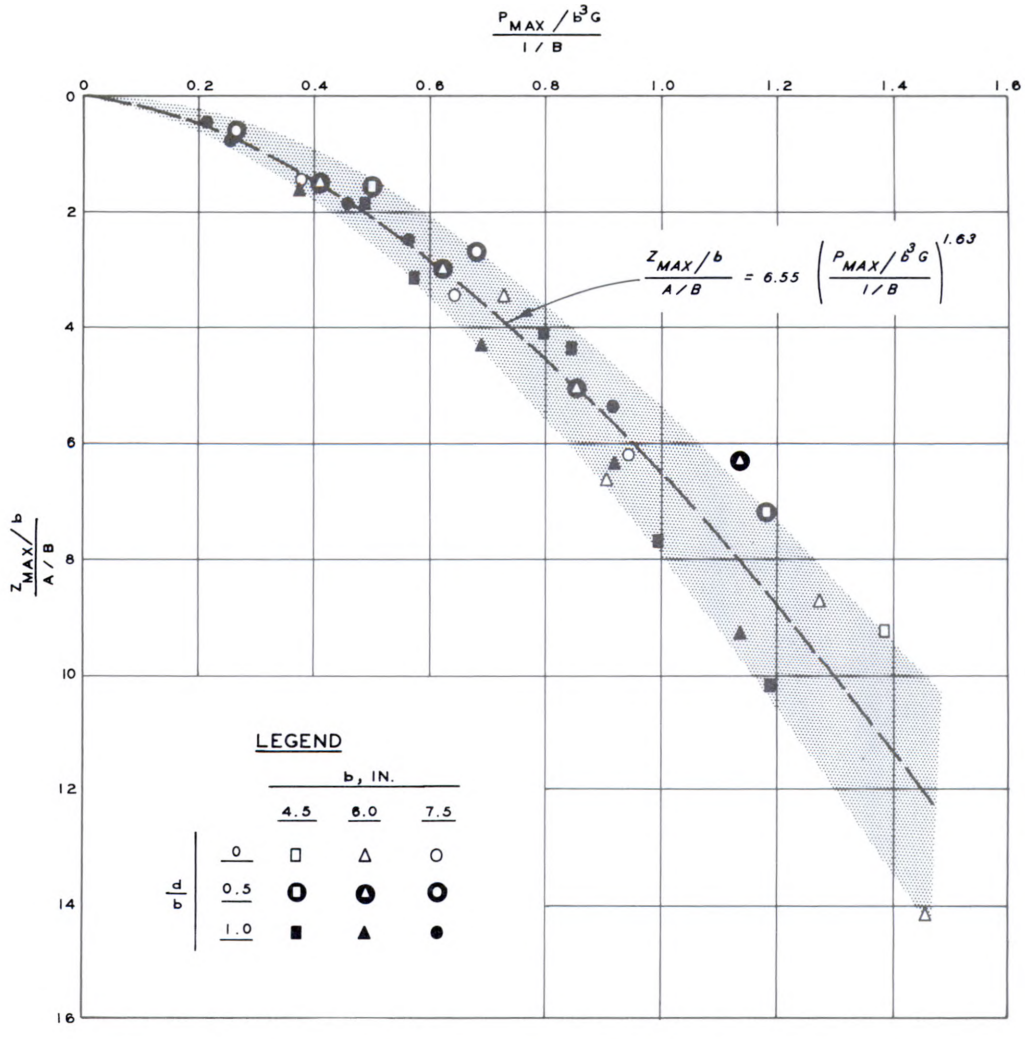

Figure 12. Normalized peak dynamic load-maximum displacement relation

of this study. The primary significance of this observation is that for a given footing-soil system and the range of variables investigated, dynamic load and displacement could be related to properties of the system determined by static test procedures. This observation further implies that the effect of depth on response of the system for the dynamic case was directly proportional to the effect of depth in the static case. The normalized dynamic load parameter is the ratio of peak dynamic load to the ultimate static reaction. The normalized dynamic displacement parameter is the ratio of maximum displacement to the pseudoelastic displacement under static loading.

Peak Dynamic Load-Time
of Maximum Displacement

No precedence nor guidance was available for normalizing load-time relations, so all probable combinations of normalizing factors were tried and results which indicate plausible relations are tabulated in Table 7 and presented in graphic form in Figure 13 (empirical curves are also shown). It was found that the peak dynamic load-time of maximum displacement relations in Figure 11a could be collapsed simply by dividing the independent load parameter $\frac{P_{max}}{b^3G}$ by the ultimate strength parameter $\frac{1}{B}$ to produce a unique relation between $\frac{\beta t(z_{max})}{T_o}$ versus $\frac{P_{max}/b^3G}{1/B}$ as shown in Figure 13a. The relations in Figures 11b and d were collapsed in a manner similar to that used for load-displacement by dividing the independent and dependent pi terms by ultimate strength and strength-stiffness ratio, respectively, to produce unique relations of $\frac{P_{max}[\beta t(z_{max})]^2/\rho b^4}{A/B}$ versus $\frac{P_{max}/b^3G}{1/B}$ shown in Figure 13b and $\frac{P_{max}[t(z_{max})]^3/mbT_o}{A/B}$ versus $\frac{P_{max}/b^3G}{1/B}$ shown in Figure 13c. When the two dependent pi terms $\frac{z_{max}}{b}$ and $\frac{g[\beta t(z_{max})]^2}{b}$ were combined, a unique relation was found to exist between the new pi term $\frac{z_{max}}{g[\beta t(z_{max})]^2}$ and $\frac{P_{max}}{b^3G}$ as presented in Figure 13d.

Empirical Relations

Empirical equations in the form of power curves for the peak dynamic load-maximum displacement and the four peak dynamic load-time of maximum displacement relations shown in Figures 12 and 13 are listed as follows:

$$\frac{z_{max}/b}{A/B} = 6.55\left(\frac{P_{max}/b^3G}{1/B}\right)^{1.63}, \qquad (10)$$

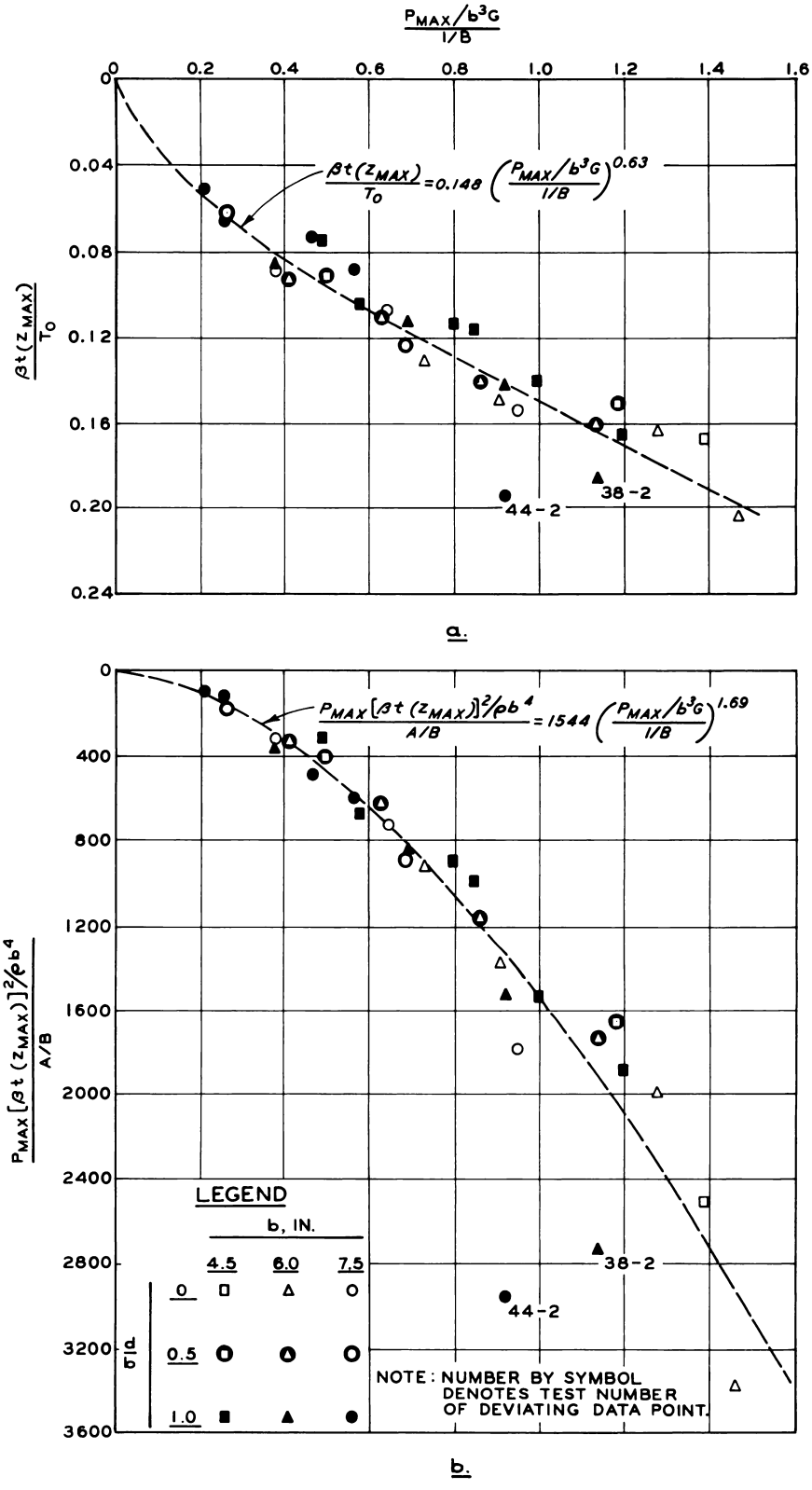

Figure 13. Normalized peak dynamic load-time of maximum displacement relations (part 1 of 2)

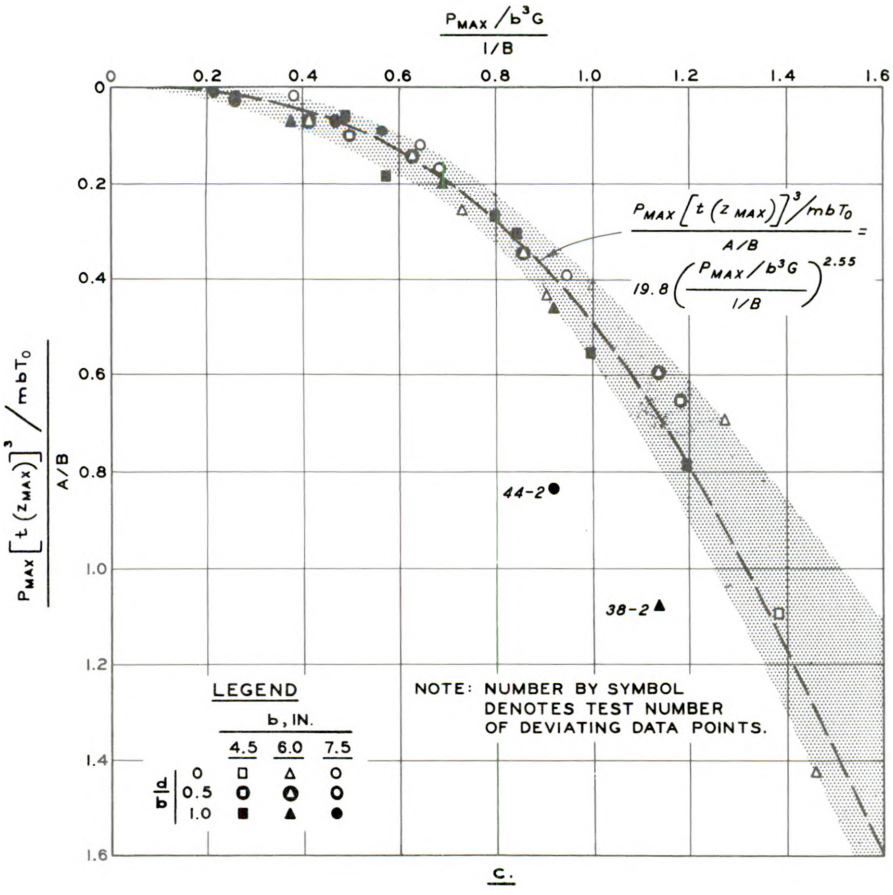

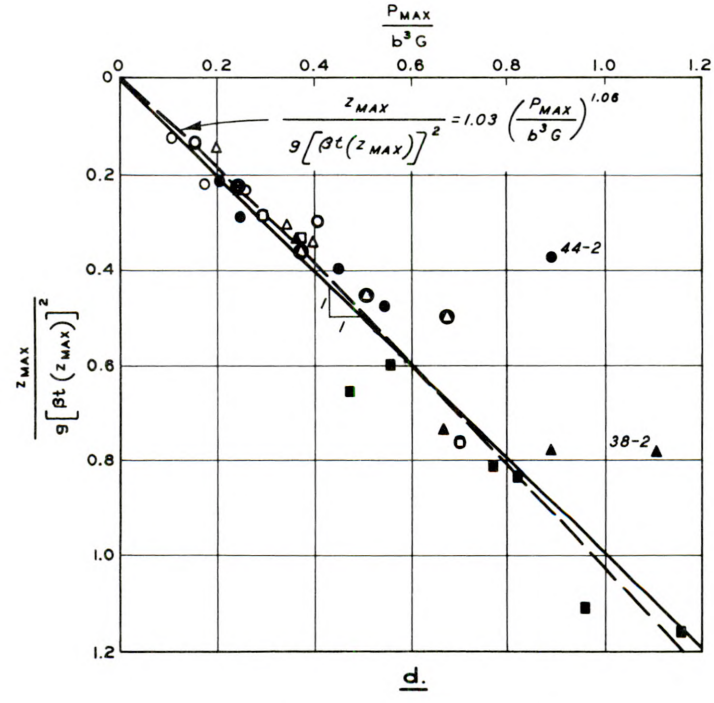

Figure 13. (part 2 of 2)

$$\frac{\beta t(z_{max})}{T_o} = 0.148 \left(\frac{P_{max}/b^3 G}{1/B} \right)^{0.63} , \tag{11}$$

$$\frac{P_{max}[\beta t(z_{max})]^2/\rho b^4}{A/B} = 1544 \left(\frac{P_{max}/b^3 G}{1/B} \right)^{1.69} , \tag{12}$$

$$\frac{P_{max}[t(z_{max})]^3/mbT_o}{A/B} = 19.8 \left(\frac{P_{max}/b^3 G}{1/B} \right)^{2.55} , \tag{13}$$

and

$$\frac{z_{max}}{g[\beta t(z_{max})]^2} = 1.03 \ (P_{max}/b^3 G)^{1.06} . \tag{14}$$

These equations represent the functional relation implied in Equations (3a)-(3e). The graphic representation of these expressions shown as curvilinear functions in Figures 12 and 13 (arithmetic plots) would plot as straight lines with logarithmic coordinates.

Earlier it was noted that two tests at $\frac{d}{b}$ of 1.0 and high peak loads, Test 44-2 (7.5-in. footing) and Test 38-2 (6-in. footing), had extended times to maximum displacement and failed to correlate with the remainder of the data. The lack of correlation is also quite evident in Figure 13. The data from these two tests were rejected on a statistical elimination basis in developing the empirical relations in Equations (10)-(14).

Equation (10) indicates that the dependent variable z_{max} varied with the peak dynamic load raised to approximately 1.6 power. This equation can be used to predict maximum displacement for similar soil and loading conditions for $\frac{d}{b}$ ratios from 0 to 1 by selecting appropriate values of $\frac{1}{B}$ and $\frac{A}{B}$ from Figure 6. However, extension to other soil conditions, e.g., a lower density sand, is not justified until the relation between footing response to dynamic loading and cone penetration resistance indicated by this study has been confirmed by further investigation in which G_s is varied over a much wider range.

Time of maximum displacement is related to maximum dynamic load by Equations (11), (12), and (13). For a given system, all the terms are constants except $t(z_{max})$, P_{max}, and T_o. Thus, these equations may be rewritten in the following form:

$$t(z_{max}) = k_1 T_o P_{max}^{0.63}, \tag{11'}$$

$$t(z_{max}) = k_2 P_{max}^{0.35}, \tag{12'}$$

and

$$t(z_{max}) = k_3 T_o^{1/3} P_{max}^{0.52}, \tag{13'}$$

where k_1, k_2, and k_3 are constants. The assumed source of loading, the nuclear weapon, imposed an interrelation between P_{max} and T_o. An approximation of this relation by a power curve over the range of values used in the model study indicated that T_o varies with approximately -0.3 power of the peak dynamic load. Substituting this relation in Equations (11') and (13'), yields the following:

$$t(z_{max}) = k_4 P_{max}^{0.33}, \tag{11''}$$

$$t(z_{max}) = k_5 P_{max}^{0.42}. \tag{13''}$$

Considering the means used to develop these expressions, Equations (12'), (11''), and (13'') are in reasonable agreement and the dependent variable $t(z_{max})$ varies with from 0.33 to 0.42 power of peak dynamic load. Thus, the cube root power may be an adequate approximation.

However, the inability to correlate Tests 38-2 and 44-2 cannot be summarily dismissed as random scatter. The atypical response of these footings during deceleration possibly indicates that the basic mechanisms controlling peak dynamic load-time of maximum displacement relations may be sensitive to footing size, peak dynamic load, and prevailing shear strength in such manner that a unique relation may not be valid over the entire range of the experimental data. While the empirical peak dynamic load-maximum displacement relation appeared to be reasonably valid over

the experimental range for load parameters up to 1.5, further investigation of the limitations on peak dynamic load-time of maximum displacement relations developed for the model study data was justified. The boundary and spacing effects studies failed to indicate significant effects on the peak dynamic load-maximum displacement relation; the additional load-time of maximum displacement data were compared with the model study curve in Appendix F of supplementary report (Poplin, 1968). On the basis of this comparison, the normalized load parameter of 0.8 appeared to be an upper limit of validity for the empirical time of maximum displacement relations for the model study data.

Equation (14) involves both dependent variables and is presented because of the inference of this relation on the effect of gravity on scaling footing response. The empirically developed constants were almost unity, and in view of the preceding assumptions the relation may be adequately expressed by:

$$\frac{z_{max}}{g[\beta t(z_{max})]^2} = \frac{P_{max}}{b^3 G} \quad , \qquad (14')$$

as shown in Figure 13d.

The special significance of the pi term $\frac{z_{max}}{g[\beta t(z_{max})]^2}$ is the similarity between this term and the Froude number used in hydrodynamic analysis. If gravity forces are significant, undistorted modeling of hydrodynamic phenomena requires the same Froude number in model and prototype. Direct comparison of footing response with hydrodynamic processes may not be entirely valid, but the existing similarity should be noted. By simple transformations, the pi term which ranges from 0.1-1.2 as shown in Figure 13d can be changed to

$$\frac{\left(\frac{v_{avg}}{\beta}\right)^2}{g z_{max}} \quad ,$$

as $\frac{z_{max}}{t(z_{max})} = v_{avg}$, the average velocity during displacement. The term given involves average velocity, but maximum velocity was about twice the

average velocity. Since peak inertial force is related to maximum velocity, using v_{max} instead of v_{avg} in the pi term would increase the numerical value by a factor of about four, but this manupulation still restricts the upper limit of this Froude numberlike pi term to less than five. If a valid comparison can be drawn, inertial forces were at least of the same order of magnitude as gravitational forces, thus, neither can reasonably be neglected. The unique relation of Equation (14) proves that approximately equal Froude numbers for each model were maintained, thereby satisfying the modeling criterion on the ratio of inertial to gravitational forces.

Work and Energy; Impulse and Momentum Relations

The preceding analysis of the test data has dealt with measured values of a single parameter. However, the indicial quantities of work, energy, impulse, and momentum which can be computed from the test data represent integral effects of several parameters over the entire response time for the system. Comparison of these quantities for the various tests aids in understanding and interpreting the fundamental behavior of the footing-soil system. Also, these values represent essential parameters useful in the evaluation of nonlinear behavior of dynamic systems. The detailed derivation of the work, energy, impulse, and momentum relations is presented in Appendix E of supplementary report, Poplin (1968) along with graphic presentation of typical data and tabulations of the computed quantities for all the dynamic tests.

Selected indicial ratios from the computations are summarized in Table 8. These ratios show that kinetic energy never comprised more than one-third of the total energy in the system at maximum velocity and maximum kinetic energy was only about 10 percent of the maximum strain energy. The primary justification for neglecting the distortion of load column mass in design and conduct of the model tests was based on the fact that when kinetic energy of the particular single-degree-of-freedom system considered is small compared with the strain energy, maximum displacement may not be significantly distorted by mass distortions (Murphy and Young, 1962). The analysis of the data has shown that maximum displacement was not distorted,

Table 8. Summary of significant work, energy, and impulse ratios

Ratio	Maximum Value	Minimum Value	Average Value
Maximum kinetic energy to external work done at time of maximum velocity	0.34	0.20	0.27
Maximum kinetic energy to maximum strain energy[a]	0.14	0.08	0.10
Impulse applied to structure at time of maximum displacement to total impulse applied to structure	0.61	0.09	0.29

[a]Maximum strain energy is also equal to total work done by the footing.

and relative values of kinetic and strain energy cited provide a satisfactory explanation of the lack of displacement distortion.

The lack of a consistent relation between impulse at maximum displacement and total impulse, demonstrated by a scatter of the ratios cited which ranged more than 50 percent, indicates that the total impulse does not provide a reliable index to the system response. This observation is further verified by comparing the actual maximum work done by the system (maximum strain energy) to the fictitious maximum work done (Norris et al., 1959). An examination of the values shows that fictitious maximum work exceeds actual work by about two orders of magnitude. Actual maximum work done was equal to no more than 5 percent of the fictitious maximum work done in any case and averaged about 1.5 percent.

Although no usable relation existed between total impulse and actual work, a comparison of maximum work done with the impulse on the structure at time of maximum displacement in Figure 14 shows a consistent relation between these parameters. For relatively small impulses, the relation is approximately quadratic but deviates for larger values. Since both of these parameters are dependent functions of maximum displacement or its time of occurrence, a relation between these quantities has limited practical use and for this reason, an empirical expression was not derived.

Dynamic Reaction-Displacement Relations

Comparison of Peak Reaction with Peak Load

This study has primarily dealt with dynamic response related to the

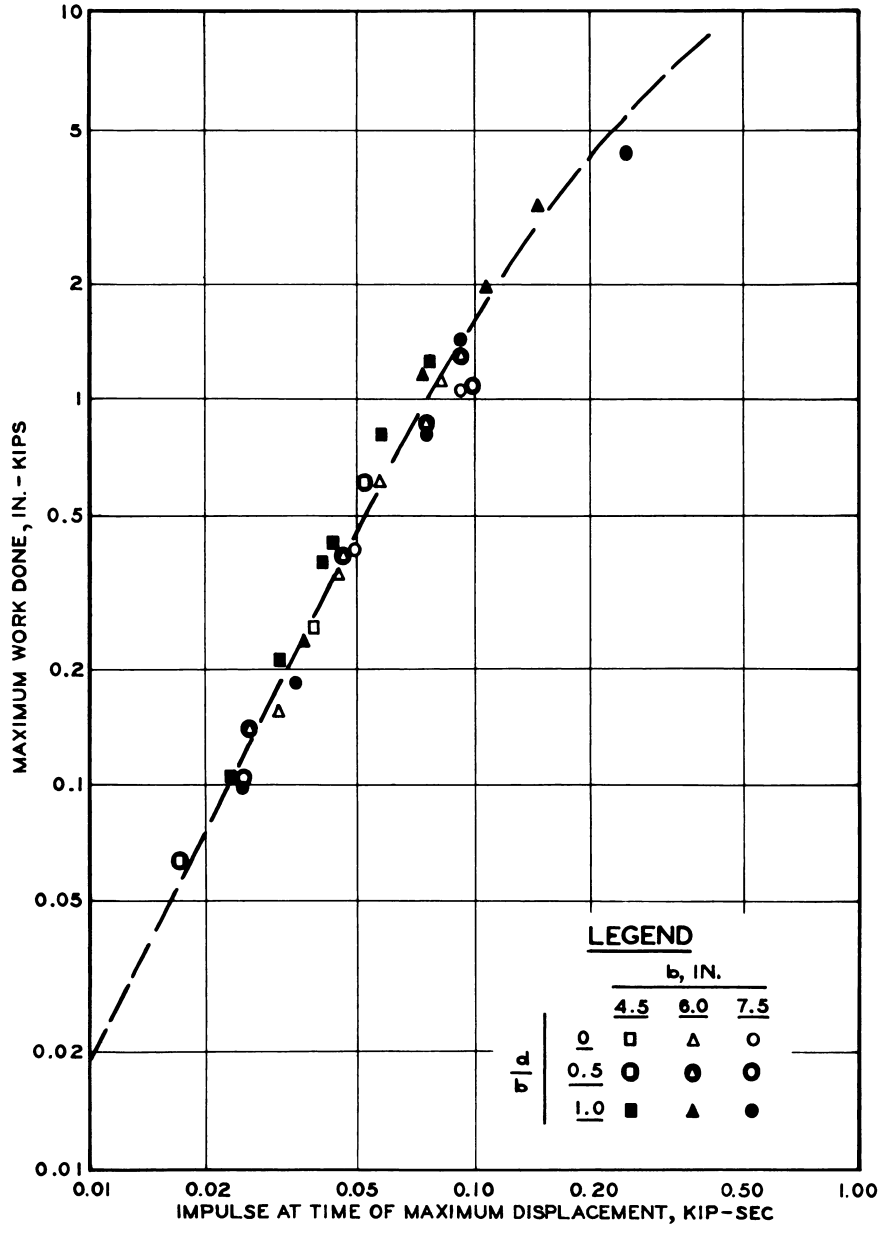

Figure 14. Comparison of work and impulse

input loading function rather than the actual footing reaction, and has shown that for a given system under a particular dynamic loading, maximum displacement can be related to the peak dynamic load. This approach was taken because the footing reaction could not be independently controlled but was kinetically dependent on the loading function and the inertial forces resulting from the response. Nevertheless, analysis of structures

under transient loading and design of foundation elements require a reasonable definition of the relation between the load acting on the footing and the resulting displacement for the prevailing conditions. In the following paragraphs, the reaction and displacement are examined. For analysis, only the dynamic reaction of that portion of reaction in excess of the initial preload was considered.

By treating the peak dynamic reaction as a dependent variable of the peak dynamic load, a plot of these parameters in the normalized form in Figure 15 shows an almost unity relation between them. Utilizing the power

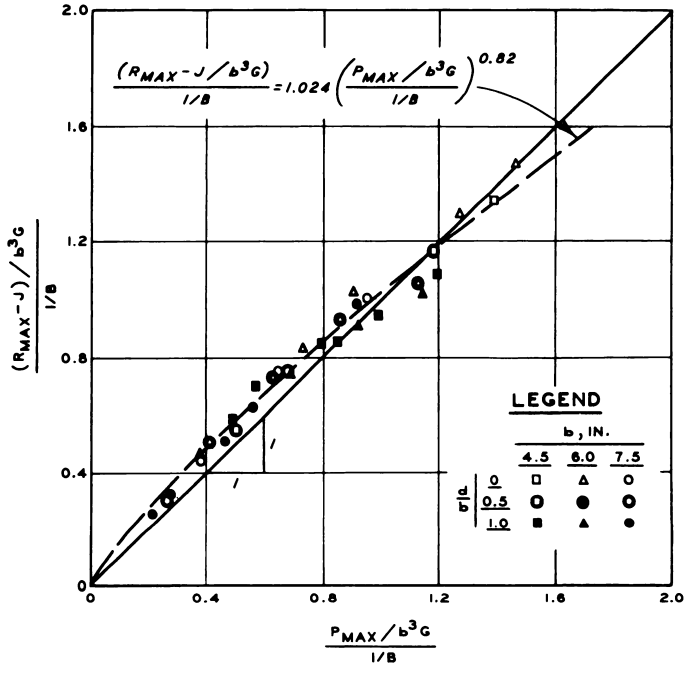

Figure 15. Comparison of peak dynamic reaction with peak dynamic load

curve-fitting procedure used earlier, the empirical relation for the model study data is

$$\frac{(R_{max} - J)/b^3G}{1/B} = 1.024\left(\frac{P_{max}/b^3G}{1/B}\right)^{0.82} . \qquad (15)$$

This relation does not deviate greatly from unity over the range of model

study data but shows that dynamic reaction tended to exceed dynamic load at lower load levels and was less than the dynamic load at higher loads. The relation developed is sufficiently consistent to permit reasonable estimates of the peak footing reaction as the basis of the applied load for the conditions tested.

The unique relation of Equation (15) also justifies developing an empirical relation to describe maximum displacement as a function of peak dynamic reaction. A plot of peak dynamic reaction versus maximum displacement in the normalized form in Figure 16 shows essentially the same

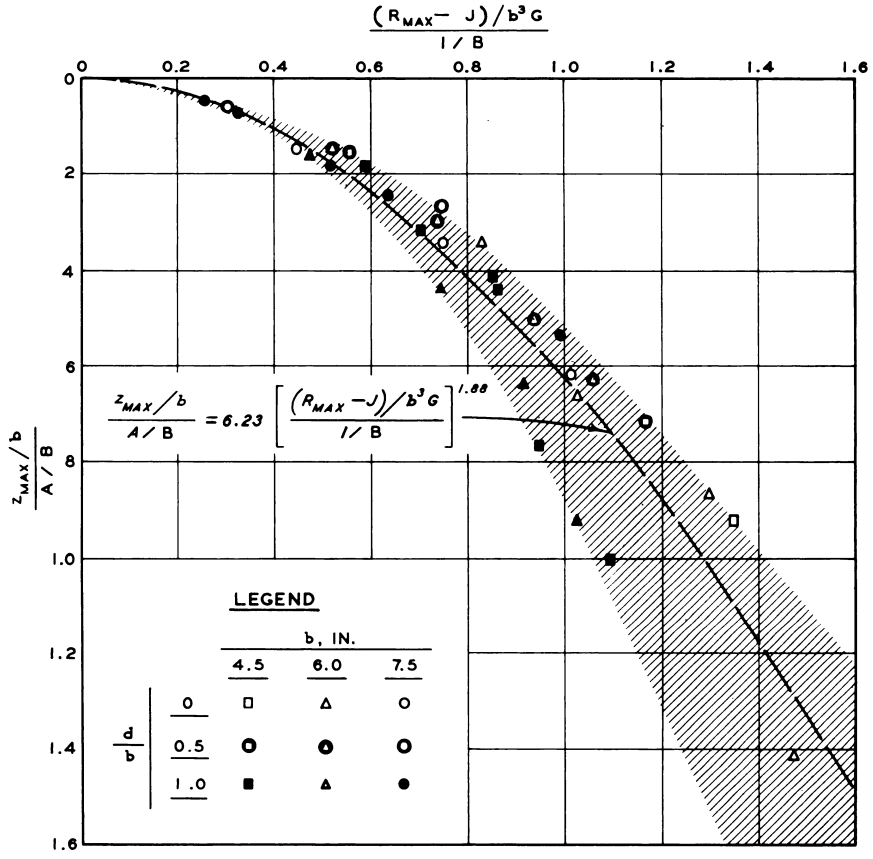

Figure 16. Normalized peak dynamic reaction-maximum displacement relation

relation as existed between peak dynamic load and maximum displacement with only a slightly greater scatter. The curve-fitting procedure yielded the empirical relation:

$$\frac{z_{max}/b}{A/B} = 6.23 \left[\frac{(R_{max} - J)/b^3 G}{1/B} \right]^{1.88} \qquad (16)$$

For a clearer comparison, all the empirical normalized load-displacement relations previously presented are shown in Figure 17.

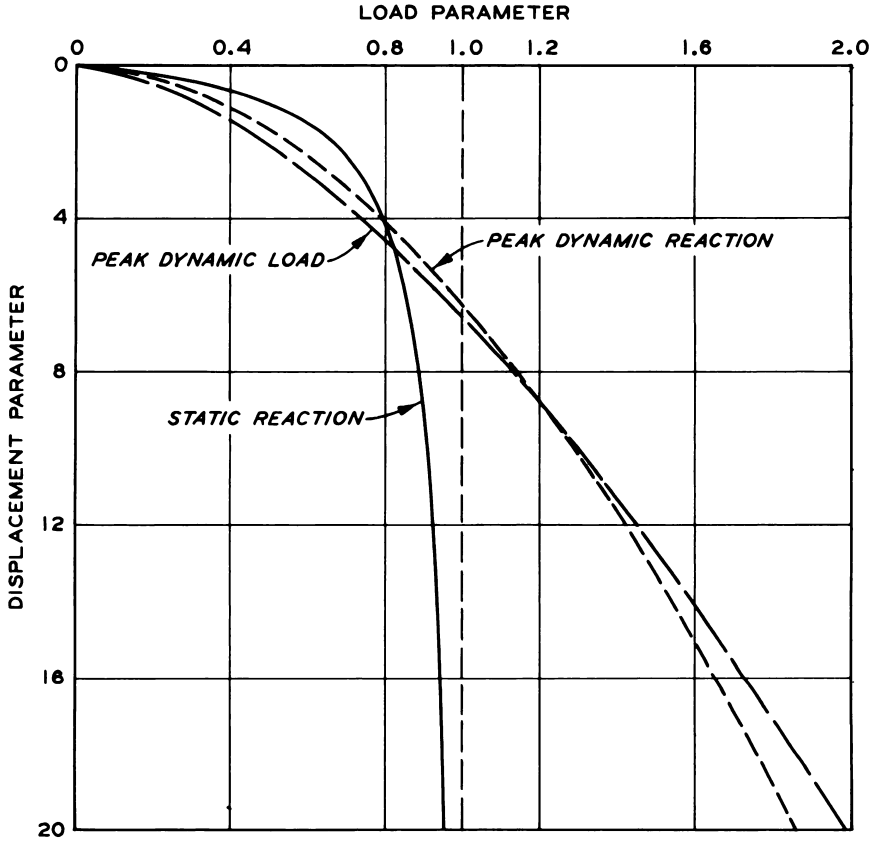

Figure 17. Empirical load-displacement relations for model study data

The two dashed curves show the relation between peak dynamic load (from Figure 12) and peak dynamic reaction (from Figure 16) versus maximum displacement. The solid curve is a continuous normalized static reaction-displacement curve (from Figure 8) applicable to the same conditions as the dynamic relations. Figure 17 clearly shows that at high load levels, the dynamically loaded footings can sustain significantly more load for a short period of time than their statically loaded counterparts.

By assuming that the peak dynamic reaction curve in Figure 17 represents an essential but unavailable relation for design of a foundation, the results of using data from other sources can be demonstrated. Displacements predicted from the peak dynamic load curve would be only slightly in error, conservative for load parameter values less than 1.2. However, the static curve would grossly underpredict maximum dynamic displacements for load parameters less than 0.8 with the largest discrepancy at about 0.6. For load parameters between 0.8 and 1.0, predictions based on the static curve would be conservative but become unrealistic as the static and dynamic curves diverge rapidly.

Reaction-Displacement Curves

Continuous nondimensional footing reaction-displacement curves of $\frac{R}{b^3G}$ versus $\frac{z}{b}$ for dynamic tests at each $\frac{d}{b}$ ratio are presented in Figures 18, 19, and 20. Rectangular hyperbolas fitted to the nondimensional static reaction-displacement data for the same soil are also shown. For this presentation, each dynamic curve was adjusted so as to originate on the static curve at a load equal to the static preload J. The effect of this adjustment was minor as the origins of the dynamic curves generally lay close to the static curve and technical problems of measuring small displacements could account for the observed deviations. Using normalizing procedures described earlier, the nondimensional curves in Figures 18, 19, and 20 were reduced to normalized form as shown in Figure 21.

Figure 21 shows that the normalized static curve provides an approximate lower bound to the dynamic test data. A curve similar in shape to the static curve but with dimensionless reaction parameters at a given dimensionless displacement equal to twice the static values would provide an approximate upper bound to all the data. In all cases the initial slopes of the dynamic reaction-displacement curves in Figure 21 are greater than the initial slope of the static curve. The dynamic increase in stiffness based on comparison of the initial portion of the test curves appears to be approximately proportional to peak dynamic load (i.e., the higher the load level, the stiffer the curve). For those cases where peak dynamic loads exceeded the ultimate static capacity (the asymptote of the static curve)

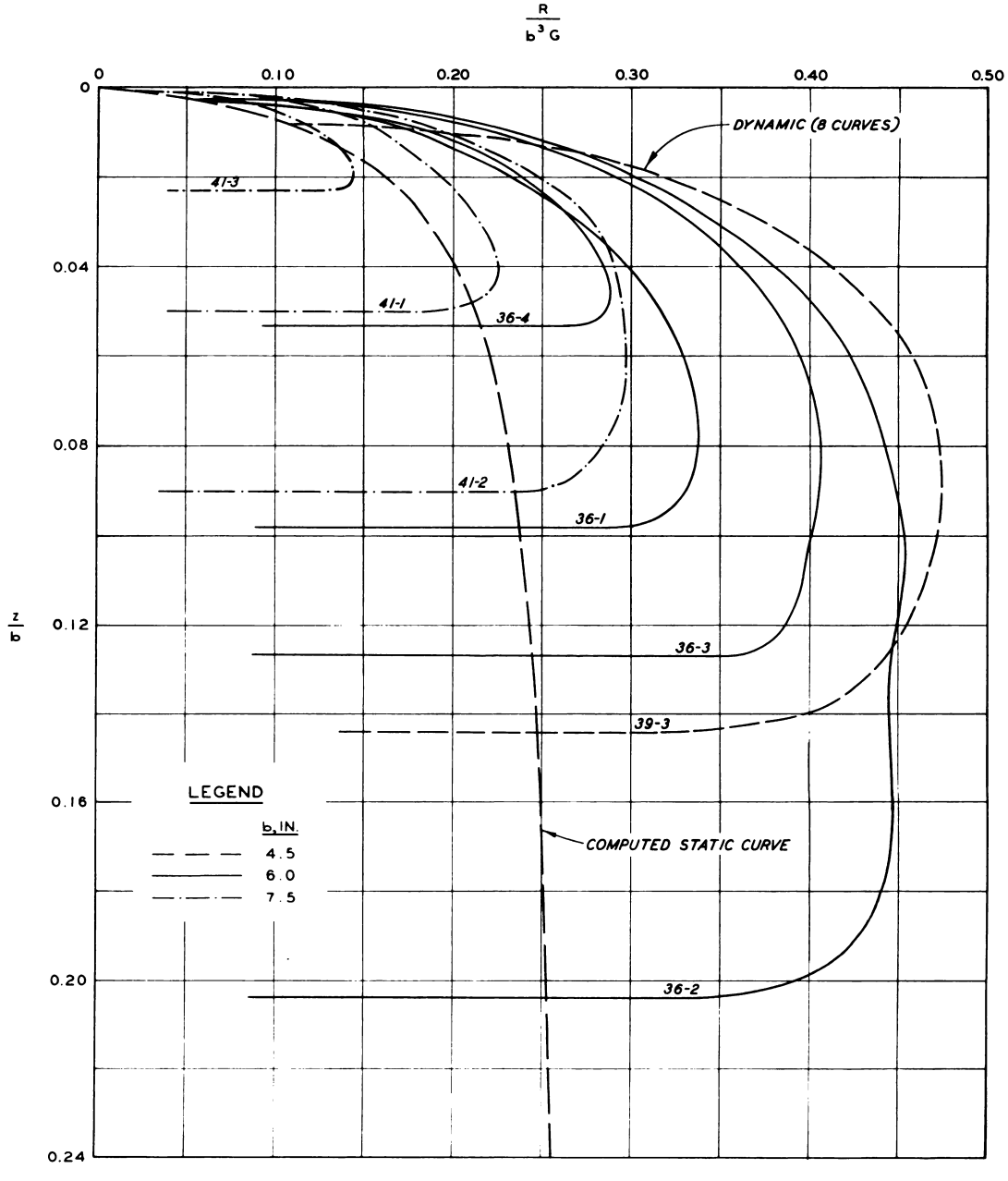

Figure 18. Nondimensional reaction-displacement curves, $\frac{d}{b} = 0$

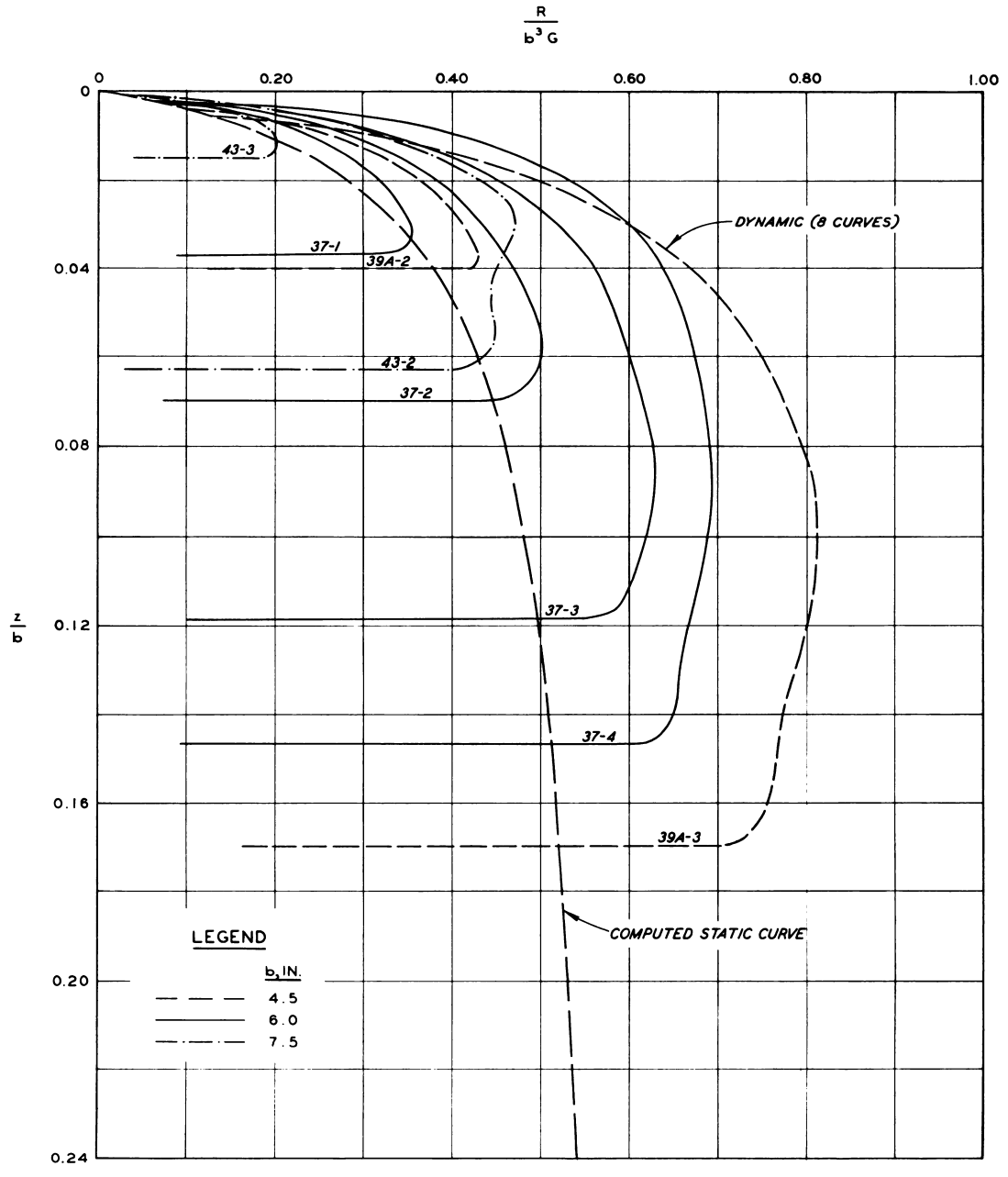

Figure 19. Nondimensional reaction-displacement curves, $\frac{d}{b} = 0.5$

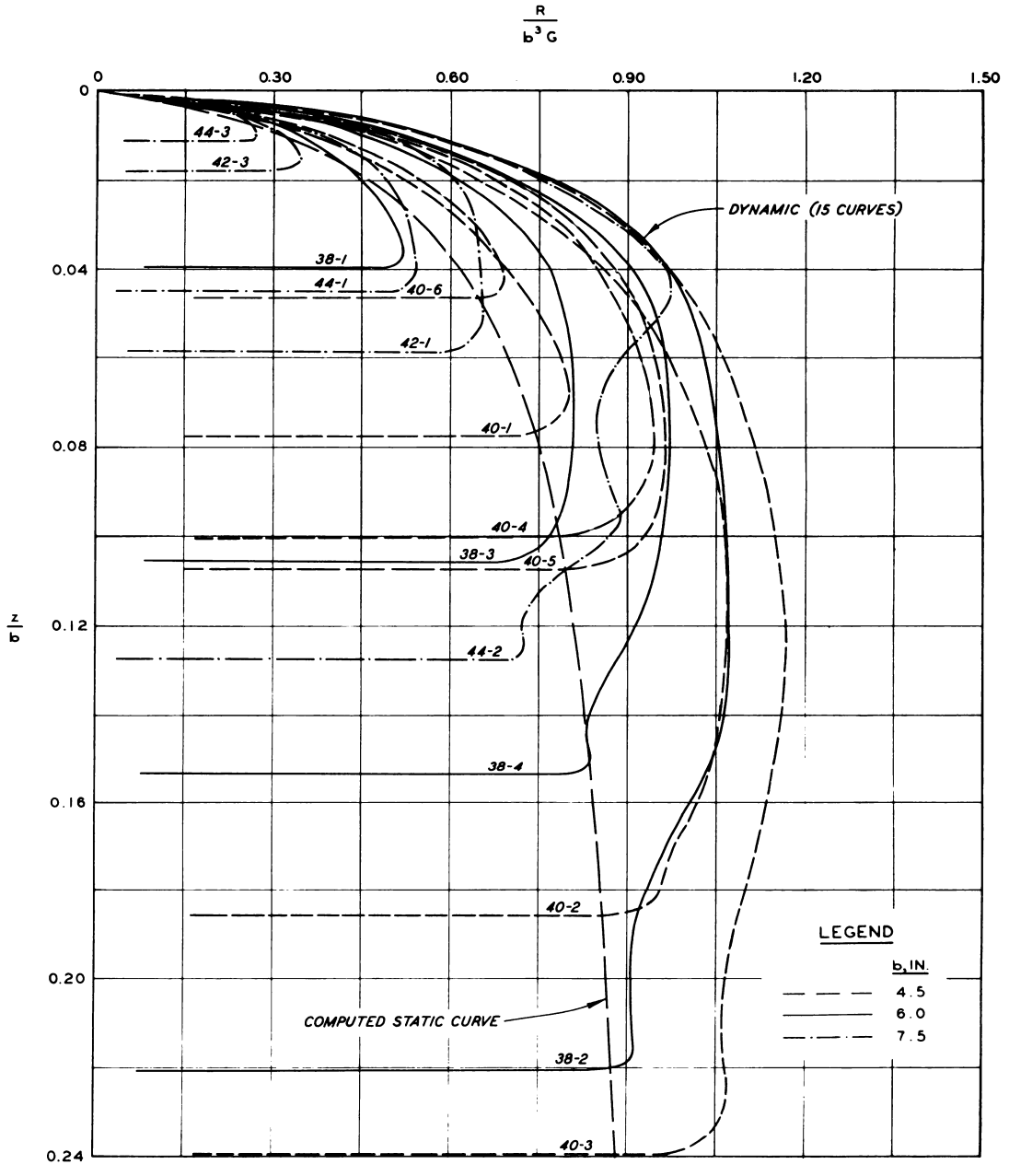

Figure 20. Nondimensional reaction-displacement curves, $\frac{d}{b} = 1.0$

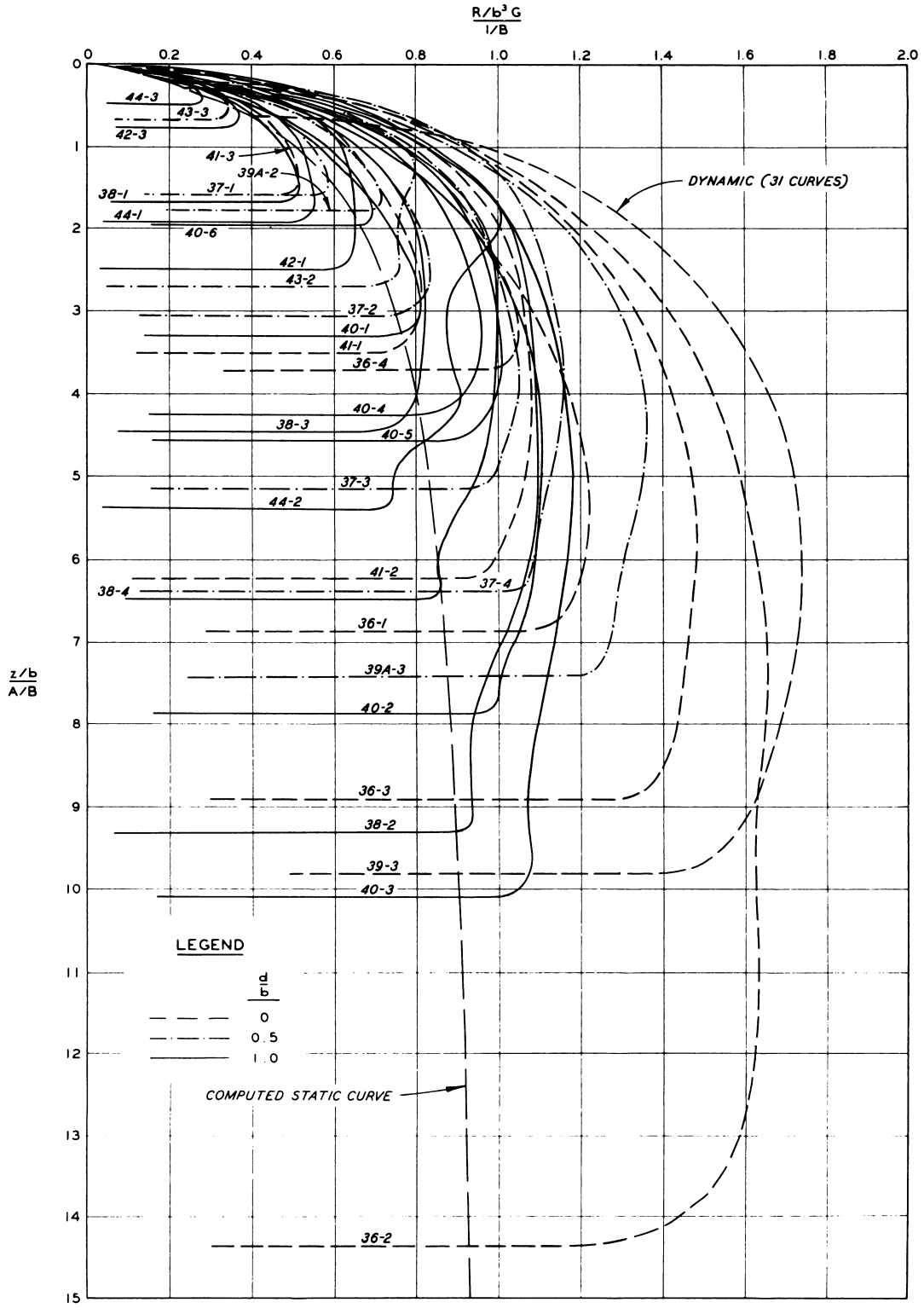

Figure 21. Normalized reaction-displacement curves

there is a general trend of significant additional displacement beyond that which occurs prior to peak reaction, accompanied by a decrease in reaction. This quasi-plastic behavior is qualitatively similar to that in a strain-controlled triaxial test on sand after failure has occurred. Possibly the ultimate load that the sand can carry has been exceeded, and continued straining occurs until the external release of the applied load brings the footing reaction down to a level which can be resisted by the sand.

Earlier, increase in depth of burial was shown to produce significantly increased footing strength (Figure 7). The curves in Figures 18, 19, and 20 show that dynamic strength indicated by the peak reaction also increased with depth of burial but at a lesser rate than for the static case. The peak dynamic reactions were almost twice the static reaction at equal displacements for surface footings but for a depth-of-burial ratio of one, the dynamic increase is only minor. The cause of the differences is not fully understood but plausible explanations based on apparent shear strength relations will be examined later.

The preceding comparative examination of the reaction-displacement curves from the model study reveal that dynamic response of footings on sand can be adequately described only by very complex functions and no simple proportionality exists between static and dynamic curves as found in the case of dynamic foundation response on clay by Jackson and Hadala (1964). A greater tendency for the dynamic curves to move back toward the static curve after reaching a peak reaction was noted as depth increased. In some cases, the dynamic reaction was less than the static reaction at the final displacement (e.g., Test 44-2, Figure 20).

In summary, dynamic loading was observed to have the effect of increasing the stiffness of reaction-displacement relations during the initial portion of the loading generally proportional to the ratio of peak dynamic load to ultimate static load, but as static stiffness or strength increased with depth of burial, the dynamic increase in initial stiffness was reduced. As the ratio of peak dynamic load to ultimate static load approached and exceeded unity, the increase in dynamic reaction at maximum displacement over static reaction was also observed to decrease as static strength increased due to the effect of confinement by the overburden.

Effect of Shear Strength on Footing Response

The foregoing analysis, particularly the reaction-displacement relations, revealed considerable strength increases due to dynamic loading. This dynamic strength increase is greater than can be explained on the basis of observed strain-rate effects in conventional strength tests in dry sand reported in the literature. It is hypothesized that the apparent strain-rate effects observed in the footing response can be attributed to the prevailing shear strength which assumes a transitory or time-dependent nature. In the following paragraphs, this hypothesis is developed and the factors that would produce time-dependent shear strength behavior are examined. There may be, however, many other factors such as dissipation of heat, changes in mode of displacement, etc., which influence response both directly and indirectly that are not specifically considered.

Shear Strength Hypothesis

The dependence of shear strength of cohesionless soil, on angle of internal friction ϕ, pore pressure u, and normal stress σ, can be expressed by Coulomb's equation in the form:

$$\tau_f(\sigma , u , \phi) = (\sigma - u) \tan \phi . \qquad (17)$$

These independent parameters are normally considered constants for static loading but may assume time-dependent characteristics under dynamic loading. Since the state of stress under a footing is largely indeterminate and by no means uniform, the effect of these variables on the footing response can be evaluated in a qualitative manner by examining the effect of a time-dependency for each parameter in turn, assuming the other two factors to remain constant.

Internal Friction Angle. The quantity $\tan \phi$ defines the effective coefficient of friction for sliding between grains, and from elementary mechanics, the coefficient of friction is dependent only on the nature of the surfaces of sliding. For ϕ to become time-dependent, dynamic loading would have to alter the nature of the intergranular contacts, but the stress levels encountered in this study were certainly insufficient to

produce fracture or crushing of sand grains, so any time-dependency of ϕ may be reasonably discounted. Rapid triaxial tests on dense, dry Ottawa sand at the Massachusetts Institute of Technology by Whitman and Healy (1962) and dynamic direct shear tests at the University of Notre Dame by Schimming et al. (1965)* indicated that changes in the internal friction angle with loading rate were minor.

Effective Normal Stress. Shear strength of cohesionless soil depends directly on the intergranular or effective normal stress acting on the plane under shear which is composed of the difference between total normal stress and the pore pressure. Under dynamic loading either the total stress or the pore pressure, or both, may assume time-dependent properties related to the deformation characteristics of the soil.

Pore Pressure. Under shearing, granular soils exhibit volumetric change tendencies. Loose sands become more compact, reducing the volume of voids, and if a pore fluid is present, pore pressure increases. Dense sands tend to dilate, causing pore pressure reductions. Under slow loading, pore pressure changes are usually dissipated by drainage, but rapid loading can conceivably cause shear to occur before dissipation takes place. In addition to the volumetric behavior of the soil, the effect of pore pressure is related to the compressibility and viscosity of the pore fluid, permeability, and length of drainage path through the soil medium. For a granular soil saturated with water, an incompressible pore fluid, small volume changes produce significant changes in pressure; whereas in the case of dry sand with air-filled voids, large volume changes are required to produce significant changes in the pressure of air, a highly compressible gas. Whenever a pressure gradient exists within a porous medium, the time required for flow to produce equalization is very short for air compared with water. While the drainage path for a surface footing test should be shorter than for a buried test, the effect of depth on pore pressure for dry sands would be only slight since drainage can also be effected into or out the surrounding medium. Isolation and quantitative assessment

---

* This reference contains an extensive historical review of the literature on time-dependent shear strength of soils.

of pore pressure effects on dynamic shear strength are particularly difficult when the pore fluid is air and represents an area that deserves further investigation. In the dynamic triaxial tests by Whitman and Healy (1962), significant pore pressures were measured when dense, saturated specimens were sheared without drainage. Dynamic direct shear tests by Schimming et al. (1965) without drainage control suggested that a dynamic strength increase in dry, dense sand could be attributed to the development of momentary negative pore pressures. One means of evaluating the effect of air pore pressure would be to conduct similar footing tests with the air evacuated from the pore spaces.

Total Normal Stress. The variables, friction angle and pore pressure, are independent of orientation since $\tan \phi$ is a scalar and u acts hydrostatically, but total normal stress, thus effective stress, varies with the orientation of the potential failure plane. Many planes of shear affect the footing response but the influence of σ can perhaps best be assessed by considering its effect on the minor principal stress plane. Heller (1964) proposed an analogy between the prism of soil beneath a footing and a triaxial test specimen where minor principal stress is derived from a lateral confining pressure. The static test results demonstrated the significant effect of minor principal stress derived from overburden in shallow burial of footings in granular soil. Heller (1964) showed that inertial stresses within the soil mass displaced by the footing constitute an effective additional confinement and analytically related the increase in minor principal stress to the vertical footing acceleration. Thus dynamic strength derived from lateral inertia of the soil can be highly transitory, having its greatest effect when the footing is experiencing initial acceleration. Also, dynamic strength from soil inertia would be expected to have a greater influence for footings on the surface and to decrease with depth since the overburden stress offers constraint against movement. In reviewing available experimental data from footing tests, Heller (1964) observed that the rate of loading of footings on the surface affected the mode of displacement of the soil under the footing quite similarly to the effect of minor principal stress from overburden on the modes of displacement under static loading. Dynamic strength from inertia could have less

effect in loose sand than in dense sand, because the footing penetration affects only a localized zone around the footing and inertial stresses are not widely distributed. In the referenced dynamic triaxial tests, the influence of lateral inertia was recognized and in the dynamic direct shear tests, an effective inertial confinement for soils that tend to dilate was observed.

Summary of Effects

In summary, the anticipated effects of dynamic loading are recapitulated:

1. The angle of internal friction is a material property independent of loading rate.
2. Pore pressures can become time-dependent if shear-induced volume changes produce corresponding pore pressure changes faster than they can be dissipated by drainage. The most significant effects are expected in dense sands that dilate upon shearing and produce negative pore pressures, resulting in a dynamic strength increase.
3. Total normal stress is time-dependent if inertial stresses are induced in the soil mass. This effect is also more significant for dense sands that tend to dilate and appear as dynamic strength increases.

On the basis of the foregoing discussion, Coulomb's equation applicable to the case of dynamically loaded footing can be written:

$$\tau_f(t) = [\sigma(t) - u(t)] \tan \phi \ , \qquad (18)$$

where the time-dependency of σ is related to the footing acceleration and the time-dependency of u is related to the permeability of the soil medium. Although both of these parametric functions exhibit their greatest effect in dense sand, the dynamic strength bonus fades very quickly through acceleration decay and rapid pore pressure equalization. The model study reaction-displacement curves in Figures 18, 19, and 20 exhibit the most significant effects of dynamic load on stiffness during the early portion of the curve, consistent with the foregoing considerations of dynamic shear strength of dry sands.

APPLICATIONS OF THE STUDY RESULTS

Implications on Modeling of Buried Structures

The physical behavior of the soil component of a foundation system is so highly dependent on constituent properties, stress history, and environmental conditions that successful application of modeling to predict response of the system requires considerable skill and possibly a little luck. The problem is further complicated for buried structures in that transient response of the foundation and the structure are integrally related. The purpose of this section is to examine the scaling rules used for this model study and to compare them with scaling rules used by other investigators in the field of protective structures.

The principles of similitude guide the selection of scale factors for length, force, and time, if all these quantities are involved in the phenomena under consideration, but do not guarantee the selection of the best combination of scale factors. Often contradictions arise and the final selection of a set of scaling rules must be based on engineering judgment and experience. Usually, very painstaking experimentation is required to prove the adequacy of a set of rules for a single given condition.

Standard terminology to describe the various scaling rules is not in general usage among investigators in the field of structure-soil systems modeling. Two of the more common scaling systems are shown in Table 9 to show the relative length, force, and time scales where n is the ratio of a characteristic length in the prototype to a characteristic length in the model.

Table 9. Comparison of scale factors

Scaling Rules	Length	Force	Time
Froude[a]	n	n^3	$\sqrt{n}$
Mach	n	n^2	n

[a]Used in this study.

There are many more ramifications of these particular scaling rules than

can be summarized, but Table 9 outlines the basic distinctions and provides a handy reference for discussion. The names used in the table are in general usage in hydrodynamic and aerodynamic modeling as Froude scaling assures kinetic similarity of inertial and gravitational forces whereas Mach scaling assures kinetic similarity of elastic and inertial forces (Lundgren, 1957; Murphy, 1950).

The scaling rules developed for the model study based on the consideration of the same cone pentration resistance gradient G and same soil mass density ρ in the model and prototype resulted in Froude scaling. While ρ was reasonably constant for the model tests, the soil strength parameter G exhibited variations; but the subsequent dimensional analysis based on the ratio of applied load to G in a nondimensional form consistent with the scaling rules indicated no distortion of maximum displacement. This development implies that identical soil properties may not be essential for adequate modeling of the response of foundation on sands. However, the range and limitations on the use of G as a modeling parameter must be determined by further investigation. Another implication arose from the study; gravity was significant in the response. Gravity could influence the system through the structural deadweight, but this was not shown to be significant in the test results. The primary influence of gravity was from the dependence of the strength of sand on the prevailing stress conditions. The static strength of the sand was dependent for the most part on the overburden stress which is directly related to gravitational forces.

Mach scaling distorts the effect of gravity but scales stress wave velocity which is essential when wave propagation and elastic response are the controlling phenomena. Murphy and Young (1962) developed Mach scaling rules for buried structure models, assuming that gravitational effects were negligible and the controlling soil parameter had the same units as pressure. In verification tests with horizontally oriented cylinders and square tubes buried in prepared specimens subjected to surface loading (drop weight and shock tube loading), distortion of strains and accelerations in the model structures in dry sand were observed. These distortions were particularly evident when the impacting drop weight produced large

vertical displacements of the soil specimen and were attributed to gravitational effects (Murphy et al., 1963; Murphy et al., 1965).

Both gravitational effects on soil strength and stiffness and wave propagation effects are significant to important protective structure problems. For the classes of structure that do not have distinct foundation elements, such as buried stiff horizontal cylinders and arches with integral floor slabs, large displacements cannot be tolerated without failures and Mach scaling may prove to be satisfactory for these cases under most conditions. However, another important category includes those structures that are designed to accept large deformation in order to mobilize available arching in the soil, thereby alleviating the load on the structure. Structures of this class are arches with strip footings and shallow-buried prismatic structures utilizing columns and spread footings. Because of the gravitational effects on the strength of cohesionless soil, Froude scaling appears to be more satisfactory for modeling the gross response of the second class of structures, whose response is interdependent on the foundation behavior when such structures are founded in cohesionless soil.

Design of Foundations

The ultimate objective of this study and related investigations of foundation response is to provide information that can be utilized by engineers to develop rational design for foundation elements and to predict the performance of these elements as related to the response of the entire structure. In the design of foundations for structures subjected to transient loading, two mutually related problems must be resolved:

1. Prevent excessive settlements.
2. Prevent detrimental contributions of the foundation to the structural response.

The first problem is quite similar to the basic problem of foundation design for static loading where the tolerable settlement is determined by the service function of the structure. However, in the case of a buried protective structure, an optimum solution to this condition may be the

worst condition for the second consideration. For example, a footing sized to minimize settlement may be excessively stiff with respect to the structure and could lead to the failure of structural elements supported by the footing. Controlled displacements during dynamic loading can significantly relieve the intensity of loading on the footing and also relieve and redistribute the loading on the structure by mobilizing active arching in the soil.

The purpose of this section is to discuss the implication of this study on the design of foundations. Since the study was restricted to a uniform dry sand with a narrow range of relative density, the findings represent small but significant contributions to the overall design problem. In the meantime, these implications should be considered only in the context of the study.

Adequacy of Foundation

The results of the model study did not indicate dynamic strength components in excess of the static strength that could be used with confidence in design foundations on sand to limit settlements. A capability of momentarily sustaining dynamically applied loads greater than the static capacity was observed; but the increased capacity was attributed, by hypothesis, to dynamic effects on effective stress which are highly transitory. This capacity diminished both as peak dynamic load and static strength increased. Therefore, modifications of the static reaction-displacement curves for use in design of footings to control settlements do not appear appropriate as the static curve represents a lower or conservative bound. However, the conservative safety factors with respect to shear failure of the footing normally used in design for conventional static loading may be relaxed, thereby permitting design for combined dead and live load up to 80 percent of the ultimate static load.

Contributions to Structural Response

Selection of a footing size does not complete the designer's task as the behavior of this footing in the overall structural complex must be ascertained. This requires performance predictions for a variety of conditions intermediate to the design conditions which cannot be based on static load-displacement curves. In Figure 17, it was shown that the static curve

underestimated maximum displacement for peak dynamic loads less than the static bearing capacity and could not be used to predict displacements for dynamic loads in excess of static capacity (i.e., dynamic load parameters greater than one).

Adequate dynamic analysis of a structure can be accomplished only when a representative resistance function is included to simulate the foundation response. The dynamic reaction-displacement curves from the model study data show these resistance functions to be nonlinear and dependent both on the static stiffness of the system and the intensity of the applied dynamic load. A fundamental requisite for an analytical resistance function is that it adequately duplicates the work done by the footing. Since most of the experimental dynamic reaction curves in Figure 21 are above the static curve, using the experimental static load-displacement without modification in an analytical model would grossly overpredict the displacement for nearly every case.

Analytical Response Predictions

An analytical prediction technique validated by experimental observation can be quite useful in studying footing response. Previous studies of dynamically loaded footings (Hadala and Jackson, 1967) have shown that response could be predicted with a single-degree-of-freedom analytical model, provided the resistance function used in the model adequately duplicates the real foundation reaction-displacement relation.

When significant strain-rate effects are present, the selection of appropriate strain-rate factors is often difficult. For footings on clay, dynamic resistance was found to be proportional to static resistance, being from 1.5 to 1.9 times greater at equal displacements (Jackson and Hadala, 1964; Hadala, 1965). However, a consistent dynamic-to-static proportionality was not observed for footings on sand in this study.

The feasibility of predicting the response of footings on sand was considered in detail in (Appendix I of supplementary report (Poplin, 1968)). Starting with the rectangular hyperbola describing static resistance, a dynamic resistance function with factors to adjust stiffness and strength

was developed. Through a numerical procedure, analytical predictions of footing response were made and compared with the observed response of four typical tests from the model study. Several analytical trials were run using adjustment factors to produce hyperbolic resistance functions that fitted the actual reaction-displacement curves.

On the basis of this comparison, the feasibility of using analytical techniques for predicting response of footings on sand was proven, but the accuracy of the predictions was sensitive to the selection and adjustment of the dynamic factors for the resistance function. The peculiar shape of the actual reaction-displacement curve after maximum displacement was difficult to fit for loads approaching or exceeding the static capacity of the footing due to the quasi-plastic behavior in that region. Further investigations along these lines utilizing more sophisticated analytical techniques could refine the accuracy of the prediction, but such efforts exceed the scope of the study.

CONCLUSIONS

As a result of the model study of dynamically loaded square footings on sand reported herein, the following conclusions are drawn:

1. The dynamic response of footings on sand can be modeled on the basis of mass density and prevailing shear strength gradient as pertinent soil properties. These conditions lead to Froude scaling rules.* Scaling of forces was found to be more critical than scaling of time. Froude scaling does not distort gravitational forces, a primary source of shear strength in sands.
2. The maximum displacement of a footing can be predicted (within the range of variables tested) provided indicial properties of the soil and foundation system are included in the computations. These properties can be determined under static conditions by cone penetration tests and plate bearing tests. Empirical relations fitted to the experimental data showed that maximum displacement was uniquely related to approximately 1.6 power of the peak dynamic load for loads ranging up to 1.5 times the ultimate static load. Similarly, time of maximum displacement was found to vary with the cube root power of peak dynamic load, valid for load up to 0.8 times the ultimate static load, but did not hold for larger loads due to a quasi-plastic behavior of the footing which extended the time of maximum displacement but did not significantly affect maximum displacement.
3. Dynamic loading produced apparent strain-rate effects in the form of increased stiffness and strength in the load-displacement relation compared to statically applied loading response. The dynamic effects were most significant during the early portion of the loading cycle but tended to diminish as displacements continued. At a given depth-of-burial to footing width ratio, the dynamic bonuses in stiffness and strength were proportional

---

* For Froude scaling, lengths scale as n, forces scale as n^3, and times scale as $\sqrt{n}$.

to the ratio of the peak dynamic load to ultimate static load. However, the dynamic bonuses were largest for footings on the surface and least for footings buried at a depth equal to their width, indicating these bonuses are inversely related to the prevailing shear strength derived from the static overburden. The apparent strain-rate effects were hypothesized to be temporary increases in shear strength related to dilatant behavior of dense sand upon shearing which increases the effective stresses both through inertial stress and pore pressure redistribution within the zone of soil influenced by the footing penetration. However, other factors not present in the static loading case and not rationally accounted for may have influenced the dynamic response.

In addition, the following conclusions are made relative to the application of study results to the design of foundation, prediction of performance, and the implications on the current state-of-the-art for investigation of dynamic response of buried structures:

1. Although dynamic effects sufficient to temporarily sustain a load in excess of the static bearing capacity of the footing were observed, the transitory nature of these effects preclude their use in design of foundations subjected to relatively long-duration impulsive loading associated with megaton range nuclear detonations. The static load-displacement curve represents a conservative bound for sizing footings to limit settlement.
2. Quantitative evaluation of the influence of foundation-structure interaction on the overall structural response can be accomplished only by including the dynamic effects in the foundation reaction-displacement relation. Analytical resistance functions can be developed which account for the dynamic increase in stiffness and strength of the foundation over values that can be observed in a static plate bearing test. Because of the apparent dependence of dynamic shear strength of sand on inertial and other transitory effects, a workable resistance function will be considerably more complex than the simple dynamic-to-static resistance ratio at equal displacements of a footing on the

surface of clay indicated in an earlier investigation.

3. Froude scaling appears more suitable for modeling the response of structural elements in sand that undergo large, nonrecoverable displacements to take advantage of load redistribution by arching and where the primary source of resistance is derived from the static overburden.

RECOMMENDATIONS FOR FURTHER RESEARCH

Future experimental and analytical studies should seek to substantiate, amplify, and extend the findings of this and preceding studies and to apply these findings toward critical problems in the design and evaluation of strategic protective structures. To accomplish these goals, consideration of the following areas of research is recommended:

1. The effects of significant parameters not intentionally varied in this study, primarily relative density and pulse duration, should be determined. If the effect of varying relative density over a practical range (70-90 percent) can be shown to have a negligible effect on the nondimensional empirical relations developed in this study, the severe limitations of identical soil in model and prototype can be discarded. Also, if using pulse durations shorter or longer than specified for the selected weapon can be shown to have a negligible effect on response, the findings of this study can be applied to systems subjected to equivalent peak loading but with different pulse durations from weapons of other yield.*
2. Investigations of the effect of foundation response on the overall structural motions of buried structure should be undertaken. A model study using arches with variable width strip footing would indicate the gross effects and yield valuable data on the load-displacement relations for entire structures. Relations developed by this recommended study should be verified by full-scale tests when and if possible.
3. Design concepts for protective structures that utilize arching within the soil often include walls supported by continuous footing. To bridge the gap between relations developed for square footings in this study and those required for continuous

---

* Parametric studies subsequent to this study to evaluate these effects have been conducted at the WES and preliminary evaluations have indicated negligible effects at most load levels.

footings, tests should be conducted with rectangular footings which reasonably approximate strip footing and the response compared with square footings of equal width.*

* WES has conducted a series of dynamic tests on 6- by 30-in. footings; the results will be reported subsequently.

Allgood, J. R., and D. A. DaDeppo. 1963. Body motion theory. Appendix A, Allgood et al., 1963.

Allgood, J. R., and R. H. Seabold. 1965. Shallow-buried arches subjected to a traveling-wave load. Technical Report No. R-375, U. S. Naval Civil Engineering Laboratory, Port Hueneme, Calif.

Allgood, J. R., C. R. White, R. F. Swalley, and H. L. Gill. 1963. Blast loading of small buried arches. Technical Report No. R-216, U. S. Naval Civil Engineering Laboratory, Port Hueneme, Calif.

Carroll, W. F. 1963. Dynamic bearing capacity of soils; Report 5, Vertical displacements of spread footings on clay: static and dynamic loading. Technical Report No. 3-599, U. S. Army Engineer Waterways Experiment Station, Vicksburg, Miss.

Cunny, R. W., and W. E. Strohm, Jr. 1963. Dynamic bearing capacity of soils - field test - the response of impulsively loaded square footings on Frenchman Flat silt. Miscellaneous Paper No. 3-572, U. S. Army Engineer Waterways Experiment Station, Vicksburg, Miss.

Dickson, W. J., and R. Yong. 1963. Principles of similitude for soil-vehicle-models. Soil Mechanics Series No. 6, McGill University, Montreal, Canada.

Fisher, W. E. 1962. Experimental studies of dynamically loaded footings on sand. University of Illinois Contract Report No. 3-52, for U. S. Army Engineer Waterways Experiment Station, Vicksburg, Miss., Contract No. DA-22-079-eng-240.

Freitag, D. R. 1965. A dimensional analysis of performance of pneumatic tires on soft soil. Technical Report No. 3-688, U. S. Army Engineer Waterways Experiment Station, Vicksburg, Miss.

Gill, H. L., and J. R. Allgood. 1964. Static loading of small buried arches. Technical Report No. R-278, U. S. Naval Civil Engineering Laboratory, Port Hueneme, Calif.

Glasstone, S. 1962. The effects of nuclear weapons. U. S. Atomic Energy Commission, U. S. Government Printing Office, Washington, D. C.

Green, A. J., J. L. Smith, and N. R. Murphy. 1964. Measuring soil properties in vehicle mobility research; Report 1, Strength-density relations of an air-dry sand. Technical Report No. 3-652, U. S. Army Engineer Waterways Experiment Station, Vicksburg, Miss.

Hadala, P. F. 1965. Dynamic bearing capacity of soils; Report 4, Investigation of a dimensionless load-displacement relation for footings on clay. Technical Report No. 3-599, U. S. Army Engineer Waterways Experiment Station, Vicksburg, Miss.

Hadala, P. F., and J. G. Jackson, Jr. 1967. An analysis of the Small Boy footing behavior. Technical Report No. 3-793, U. S. Army Engineer Waterways Experiment Station, Vicksburg, Miss.

Heller, L. W. 1964. Failure modes of impact-loaded footings on dense sand. Technical Report No. R-281, U. S. Naval Civil Engineering Laboratory, Port Hueneme, Calif.

Jackson, J. G., Jr., and P. F. Hadala. 1964. Dynamic bearing capacity of soils; Report 3, The application of similitude to small-scale footing tests. Technical Report No. 3-599, U. S. Army Engineer Waterways Experiment Station, Vicksburg, Miss.

Johnson, T. D., and H. O. Ireland. 1963. Tests on clay subsoils beneath statically and dynamically loaded spread footings. University of Illinois Contract Report No. 3-74, for U. S. Army Engineer Waterways Experiment Station, Vicksburg, Miss., Contract No. DA-22-079-eng-240.

Khachaturian, N. 1959. Report on survey of literature in connection with dynamic bearing capacity of soils. University of Illinois Contract Report No. 3-38, for U. S. Army Engineer Waterways Experiment Station, Vicksburg, Miss., Contract No. DA-22-079-eng-240.

Kondner, R. L., and R. J. Krizek. 1962. Correlation of load bearing tests on soils. Proceedings, Highway Research Board, Washington, D. C., Vol. 41.

Langhaar, H. L. 1951. Dimensional Analysis and Theory of Models. John Wiley and Sons, Inc., New York, N. Y.

Lundgren, H. 1957. Dimensional analysis in soil mechanics. Civil Engineering and Building Construction Series, Vol. 4, No. 10, Acta Polytechnica 237.

Milovic, D. M. 1965. Comparison between the calculated and experimental values of ultimate bearing capacity. Proceedings, Sixth International Conference on Soil Mechanics and Foundation Engineering, Montreal, Canada, Vol. 3, 142-144.

Murphy, G. 1950. Similitude in Engineering. The Ronald Press, New York, N. Y.

Murphy, G., and D. F. Young. 1962. A study of the use of models to simulate dynamically loaded underground structures. Iowa State University Technical Documentary Report No. AFSWC-TDR-62-2, for U. S. Air Force Special Weapons Center (now Air Force Weapons Laboratory), Kirtland Air Force Base, N. Mex., Contract AF 29(601)-4375.

Murphy, G., D. F. Young, and C. W. Martin. 1963. Use of models to predict the dynamic response of dynamically loaded underground structures. Iowa State University Technical Documentary Report No. RTD-TDR-63-3064, for U. S. Air Force Weapons Laboratory, Kirtland Air Force Base, N. Mex., Contract No. 29(601)-5359.

Murphy, G., D. F. Young, and K. G. McConnell. 1965. Similitude of dynamically loaded buried structures. Iowa State University Technical

Report No. WL-TR-64-142, for U. S. Air Force Weapons Laboratory, Kirtland Air Force Base, N. Mex., Contract No. AF29(601)-5359.

Murphy, N. R. 1965. Measuring soil properties in vehicle mobility research; Report 2, An evaluation of the rectangular hyperbola for describing the load-deformation response of soils. Technical Report No. 3-652, U. S. Army Engineer Waterways Experiment Station, Vicksburg, Miss.

Norris, C. H., R. J. Hansen, M. J. Holley, Jr., J. M. Biggs, S. Namyet, and J. K. Minami. 1959. Structural Design for Dynamic Loads. McGraw-Hill Book Company, Inc., New York, N. Y.

Plantema, G. 1957. Influence of density on sounding results in dry, moist, and saturated sands. Proceedings, Fourth International Conference on Soil Mechanics and Foundation Engineering, London, Vol. 1, 237-240.

Poplin, J. K. 1965a. Dynamic bearing capacity of soils; Report 2, Dynamically loaded small-scale footing tests on dry, dense sand. Technical Report No. 3-599, U. S. Army Engineer Waterways Experiment Station, Vicksburg, Miss.

Poplin, J. K. 1968. A model study of dynamically loaded square footings on dry sand. Supplement, Appendixes A-J. Technical Report No. S-69-3, U. S. Army Engineer Waterways Experiment Station, Vicksburg, Miss.

Roberts, J. E. 1961. Small-scale footing studies: a review of the literature. Appendix B for preliminary design study for a dynamic soil testing laboratory. Massachusetts Institute of Technology Technical Report No. AFSWC-TR-61-48, for U. S. Air Force Special Weapons Center (now Air Force Weapons Laboratory), Kirtland Air Force Base, N. Mex., Contract No. AF29(601)-1947.

Sager, R. A. 1965. Concrete arch studies; project 3.2 Operation Snowball. Miscellaneous Paper No. 1-736, U. S. Army Engineer Waterways Experiment Station, Vicksburg, Miss.

Schimming, B. B., H. J. Haas, and H. C. Saxe. 1965. A comparison of the dynamic and static shear strengths of cohesionless, cohesive and combined soils. University of Notre Dame Technical Report No. AFWL TR-65-48, for U. S. Air Force Weapons Laboratory, Kirtland Air Force Base, N. Mex., Contract No. AF29(601)-5174.

Selig, E. T., and K. E. McKee. 1961. Static and dynamic behavior of small footings. Proceedings, ASCE, Journal of the Soil Mechanics and Foundations Division, Vol. 87, SM6, 29-47.

Sloan, R. C. 1962. Dynamic bearing capacity of soils; Report 1, Dynamic loading machine and preliminary small-scale footing tests. Technical Report No. 3-599, U. S. Army Engineer Waterways Experiment Station, Vicksburg, Miss.

Taylor, D. W. 1948. Fundamentals of Soil Mechanics. John Wiley and Sons, Inc., New York, N. Y.

Tener, R. K. 1964. Model study of a buried arch subjected to dynamic loading. Technical Report No. 1-660, U. S. Army Engineer Waterways Experiment Station, Vicksburg, Miss.

Terzaghi, K. 1955. Evaluation of coefficients of subgrade reaction. Geotechnique, Vol. 5, 297-326.

Triandafilidis, G. E. 1961. Analytical study of dynamic bearing capacity of foundations. University of Illinois Contract Report No. 3-45, for U. S. Army Engineer Waterways Experiment Station, Vicksburg, Miss., Contract No. DA-22-079-eng-240.

Wallace, W. L. 1961. Theoretical study of the displacement of long footings by dynamic loads. Miscellaneous Paper No. 3-418, U. S. Army Engineer Waterways Experiment Station, Vicksburg, Miss.

White, C. R. 1964a. Static and dynamic plate-bearing tests on sand without overburden. Technical Report No. R-277, U. S. Naval Civil Engineering Laboratory, Port Hueneme, Calif.

White, C. R. 1964b. Static and dynamic plate-bearing tests on sand with overburden. Technical Report No. R-338, U. S. Naval Civil Engineering Laboratory, Port Hueneme, Calif.

Whitman, R. V., and K. A. Healy. 1962. The response of soils to dynamic loadings; Report 9, Shearing resistance of sands during rapid loadings. Massachusetts Institute of Technology Contract Report No. 3-26, for U. S. Army Engineer Waterways Experiment Station, Vicksburg, Miss., Contract No. DA-22-079-eng-224.

Whitman, R. V., and U. Luscher. 1965. Footings for protective structures. Professional Paper No. P65-7, Massachusetts Institute of Technology, Cambridge, Mass.

DISTRIBUTION LIST

Address	No. of Copies
Army	
Chief of Engineers, Department of the Army	
ATTN: ENGTE-E	2
ENGCW-E	1
ENGMC-E	1
ENGAS-I	1
ENGCW-Z	1
ENGMC-DE	1
ENGTE-M	1
ENGTE-P	1
Washington, D. C. 20315	
Mr. L. Schindler	1
Office, Chief of Engineers (ENGMC-EM)	
Department of the Army	
Washington, D. C. 20315	
Division Engineer, U. S. Army Engineer Divisions (one copy to each)	10
Continental United States	
Division Engineer	
U. S. Army Engineer Division, Huntsville	
ATTN: Mr. T. R. Wathen	1
Mr. G. T. Mahoney	1
Mr. H. O. Baker	1
P. O. Box 1600, West Station	
Huntsville, Alabama 35807	
District Engineer, U. S. Army Engineer District, Omaha	1
6012 U. S. Post Office and Court House	
215 North 17th Street	
Omaha, Nebraska 68101	
Commanding General, Aberdeen Proving Ground	4
ATTN: Director, Ballistic Research Laboratories	
Aberdeen, Maryland 21005	
Commandant, Army War College	1
ATTN: Library	
Carlisle Barracks, Pennsylvania 17013	

Address	No. of Copies

Army (Continued)

Commanding General, The Engineer Center ATTN: Assistant Commandant, Engineer School Fort Belvoir, Virginia 22060	1
Director of Civil Defense, Office of the Secretary of the Army ATTN: Shelter Research Division Engineering Development Division (Research Directorate) Architectural and Engineering Development Division (Technical Services Directorate) Mr. George Sisson (RE-ED) Washington, D. C. 20310	 1 1 1 2
Chief of Research and Development, Department of the Army ATTN: Atomic Office CRDES Washington, D. C. 20310	 1 1
Commanding Officer, Picatinny Arsenal ATTN: ORDBB-TK Dover, New Jersey 07801	1
Chief of Research and Development, Headquarters, Department of the Army ATTN: Director of Army Technical Information Washington, D. C. 20310	3 copies of Form 1473
Director, Special Weapons Development, Hq, CDC ATTN: Chester I. Peterson Fort Bliss, Texas 79906	1
President, U. S. Army Air Defense Board Fort Bliss, Texas 79906	1
Commandant, U. S. Army Air Defense School Fort Bliss, Texas 79906	1
Commanding Officer, U. S. Army Combat Developments Command Air Defense Agency Fort Bliss, Texas 79916	1
Commanding Officer, U. S. Army Combat Developments Command Artillery Agency Fort Sill, Oklahoma 73504	1

Address	No. of Copies

Army (Continued)

Commanding Officer, U. S. Army Combat Developments Command Chemical-Biological-Radiological Agency Fort McClellan, Alabama 36205	1
Commanding Officer, U. S. Army Combat Developments Command Combined Arms Agency Fort Leavenworth, Kansas 66027	1
Commanding Officer, U. S. Army Combat Developments Command Engineer Agency Fort Belvoir, Virginia 22060	1
Commanding Officer, U. S. Army Combat Developments Command Institute of Nuclear Studies Fort Bliss, Texas 79916	1
Commanding Officer, U. S. Army Combat Developments Command Medical Service Agency Fort Sam Houston, Texas 78234	1
Commanding Officer, U. S. Army Combat Developments Command Ordnance Agency, Aberdeen Proving Ground Aberdeen, Maryland 21005	1
Commanding General, U. S. Army Combat Developments Command Service Support Group Fort Lee, Virginia 23801	1
Commanding Officer, U. S. Army Combat Developments Command Transportation Agency Fort Eustis, Virginia 23604	1
Director, Nuclear Cratering Group U. S. Army Corps of Engineers Lawrence Radiation Laboratory P. O. Box 808 Livermore, California 94550	1
Commanding General, U. S. Army Materiel Command ATTN: AMCRD-DE-N Washington, D. C. 20310	2

Address	No. of Copies

Army (Continued)

Commanding General, U. S. Army Missile Command Huntsville, Alabama 35809	1
Director, U. S. Army Mobility Equipment Research and Development Center ATTN: Chief, Technical Support Branch Fort Belvoir, Virginia 22060	1

Navy

Chief of Naval Research, Navy Department ATTN: Code 811 Washington, D. C. 20390	1
Commanding Officer, U. S. Naval Civil Engineer Corps Officer School U. S. Naval Construction Battalion Center Port Hueneme, California 93041	1
Commanding Officer & Director U. S. Naval Civil Engineering Laboratory	
ATTN: Library	1
Dr. Warren A. Shaw	1
Mr. J. R. Allgood	1
Mr. C. R. White	1
Port Hueneme, California	
Director, U. S. Naval Research Laboratory Washington, D. C. 20390	1

Air Force

Air Force Weapons Laboratory	
ATTN: Library	4
WLDC	1
Dr. H. F. Cooper, Jr.	1
1LT J. L. Bratton	1
Kirtland AFB, New Mexico 87117	

Address	No. of Copies

Air Force (Continued)

Space and Missile Systems Organization	
ATTN: Code SMNP	1
Code SAMSO (SMQNM)	1
Norton Air Force Base	
San Bernardino, California 92409	
Director of Civil Engineering	1
Headquarters, USAF	
ATTN: AFOCE	
Washington, D. C. 20330	
Director of Research and Development	1
DCS/D, Headquarters, USAF	
ATTN: Guidance & Weapons Division	
Washington, D. C. 20330	
Director, U. S. Air Force Project RAND	
Via: U. S. Air Force Liaison Office	
The RAND Corporation, 1700 Main Street	
ATTN: Library	1
Dr. Harold Brode	1
Dr. Olen A. Nance	1
Santa Monica, California 90406	

Universities

Duke University	1
Professor Aleksander B. Vesic	
Department of Civil Engineering	
Durham, North Carolina 27706	
Georgia Institute of Technology	1
Dr. B. B. Mazanti	
School of Civil Engineering	
Atlanta, Georgia 30332	
University of Illinois, Department of Civil Engineering	
ATTN: Professor A. J. Hendron, Jr.	1
Professor N. M. Newmark	1
Urbana Campus	
Urbana, Illinois 61803	

Address	No. of Copies

Universities (Continued)

Louisiana State University Dr. J. K. Poplin Department of Civil Engineering Baton Rouge, Louisiana 70803	1
The University of Michigan Department of Civil Engineering ATTN: Professor F. E. Richart, Jr. Dr. J. R. Hall, Jr. Ann Arbor, Michigan 48104	 1 1
University of New Mexico Eric H. Wang Civil Engineering Research Facility ATTN: Mr. P. Abbott Mr. Delmar E. Calhoun Dr. G. Triandafilidis Dr. Eugene Zwoyer P. O. Box 188, University Station Albuquerque, New Mexico 87106	 1 1 1 1
North Carolina State University Professor Ralph E. Fadum Box 5628 Raleigh, North Carolina 27607	1
University of Notre Dame Dr. H. C. Saxe Department of Civil Engineering South Bend, Indiana 46615	1

Other

Director, Advanced Research Projects Agency ATTN: NTDO Washington, D. C. 20301	1
Aerospace Corporation ATTN: Dr. S. B. Batdorf Dr. M. B. Watson 1111 E. Mill Street San Bernardino, California 92408	 1 1

Address	No. of Copies

Other (Continued)

Agbabian-Jacobsen Associates, Engineer Consultants 8939 South Sepulveda Boulevard, Suite 340 Los Angeles, California 90045	1
The Boeing Company, Aerospace Group Missile and Information Systems Division ATTN: Mr. Robert W. Hager Mr. H. G. Leistner Mr. Ken Levien P. O. Box 3985 Seattle, Washington 98124	 1 1 1
Director, Defense Atomic Support Agency ATTN: SPSS Washington, D. C. 20301	5
Defense Documentation Center (DDC) ATTN: Mr. Myer Kahn Cameron Station Alexandria, Virginia 22314 (NO TOP SECRET TO THIS ADDRESS)	20
Director, Defense Intelligence Agency ATTN: DIAAP-IK2 Washington, D. C. 20301	1
Director of Defense Research and Engineering ATTN: Technical Library Washington, D. C. 20301	1
Defence Research Establishment, Suffield Ralston, Alberta, Canada	1
Denver Mining Research Center ATTN: Dr. Leonard A. Obert Building 20, Denver Federal Center Denver, Colorado 80225	1
Mr. John Foss Outside Structures Department Bell Telephone Laboratories Whippany, New Jersey	1

Address	No. of Copies

Other (Continued)

IIT Research Institute	
ATTN: Library	1
Dr. E. Vey	1
Chicago, Illinois 60616	
Massachusetts Institute of Technology	
Division of Sponsored Research	
ATTN: Dr. Robert J. Hansen	1
Dr. Robert V. Whitman	1
77 Massachusetts Avenue	
Cambridge, Massachusetts 02139	
Manager, Nevada Operations Office	1
USAEC, Box 1676	
Las Vegas, Nevada 89101	
Sandia Corporation	1
ATTN: Classified Document Division for Dr. M. L. Merritt	
P. O. Box 5800	
Albuquerque, New Mexico 87115	
Stanford Research Institute	
ATTN: Library	1
Dr. E. G. Chilton	1
Mr. Fred M. Sauer	1
Menlo Park, California 94025	
TRW Systems	
ATTN: Dr. Millard V. Barton	1
Mr. Jerry Carpenter	1
Mr. Norman Lipner	1
Mr. Phil H. Huff	1
One Space Park	
Redondo Beach, California 90278	
URS Corporation	1
ATTN: Mr. Harold Mason	
1811 Trousdale Drive	
Burlingame, California 94010	
U. S. Documents Officer	1
Officer of the United States National Military Representative-SHAPE	
APO New York, New York 09055	

Address	No. of Copies

Other (Continued)

Mr. G. F. Weissmann Room 1B-124, Bell Telephone Laboratories Murray Hill, New Jersey 07971	1
Mr. Stanley D. Wilson Shannon and Wilson, Inc. 1105 North 38th Street Seattle, Washington 98103	1

Unclassified

Security Classification

DOCUMENT CONTROL DATA - R & D

(Security classification of title, body of abstract and indexing annotation must be entered when the overall report is classified)

1. ORIGINATING ACTIVITY (Corporate author)	2a. REPORT SECURITY CLASSIFICATION
U. S. Army Engineer Waterways Experiment Station Vicksburg, Mississippi	Unclassified
	2b. GROUP

3. REPORT TITLE

A MODEL STUDY OF DYNAMICALLY LOADED SQUARE FOOTINGS ON DRY SAND; SUPPLEMENT, APPENDIXES A-J (on file in USAEWES Research Center Library)

4. DESCRIPTIVE NOTES (Type of report and inclusive dates)

Final report

5. AUTHOR(S) (First name, middle initial, last name)

Jack K. Poplin

6. REPORT DATE	7a. TOTAL NO. OF PAGES	7b. NO. OF REFS
March 1969	93	44

8a. CONTRACT OR GRANT NO.	9a. ORIGINATOR'S REPORT NUMBER(S)
b. PROJECT NO.	Technical Report S-69-3
c.	9b. OTHER REPORT NO(S) (Any other numbers that may be assigned this report)
d.	

10. DISTRIBUTION STATEMENT

This document has been approved for public release and sale; its distribution is unlimited.

11. SUPPLEMENTARY NOTES	12. SPONSORING MILITARY ACTIVITY
	Defense Atomic Support Agency Office, Chief of Engineers, U. S. Army

13. ABSTRACT

The investigation reported herein was undertaken to develop an approach to modeling displacements of surface and shallow-buried footings on dry sand subject to high-intensity, single-pulse loads. A hypothetical shallow-buried structure with an isolated footing loaded by airblast overpressure produced by detonation of a nuclear weapon was assumed for design of load pulses on nine model footings used: footing widths of 4.5, 6.0, and 7.5 in. and depth-of-burial to footing width ratios of 0, 0.5, and 1.0. The principles of similitude were used to scale length, force, and time in the models. The models were placed in mobile test bins of uniform, fine, dry sand (90 percent relative density) and subjected to dynamic and static loading. Nondimensional load-displacement relations dependent only on depth-of-burial ratio were developed relating maximum displacement to peak dynamic load, footing width, and soil shear strength gradient. When the dynamic response of the footings in the form of reaction-displacement curves was compared with static response, an increase in initial stiffness and ultimate strength was observed for dynamic loading. However, these dynamic increases were greatest when the static shear strength was lowest, i.e. footings on the surface, and were least for footings buried at a depth equal to its width where the static overburden produced a substantial increase in shear strength.

DD FORM 1 NOV 68 1473 REPLACES DD FORM 1473, 1 JAN 64, WHICH IS OBSOLETE FOR ARMY USE.

Unclassified

Security Classification

14. KEY WORDS	LINK A		LINK B		LINK C	
	ROLE	WT	ROLE	WT	ROLE	WT
Dynamic loads						
Footings						
Models						
Sands						
Static loads						
Subsurface structures